Hydro-morphological effects of bridge-crossings on large braided/anabranched sand-bed rivers

Akram, Muhammad Rizwan; Khan, Muzaffar; Crosato, Alessandra

DOI
10.1080/23249676.2024.2410884

Publication date
2024

Document Version
Final published version

Published in
Journal of Applied Water Engineering and Research

Citation (APA)
Akram, M. R., Khan, M., & Crosato, A. (2024). Hydro-morphological effects of bridge-crossings on large braided/anabranched sand-bed rivers. *Journal of Applied Water Engineering and Research*, *13*(1), 59-80. https://doi.org/10.1080/23249676.2024.2410884

JOURNAL OF APPLIED WATER ENGINEERING AND RESEARCH
https://doi.org/10.1080/23249676.2024.2410884

Taylor & Francis
Taylor & Francis Group

CASE REPORT

Hydro-morphological effects of bridge-crossings on large braided/anabranched sand-bed rivers

Muhammad Rizwan Akram[a], Muzaffar Khan[a] and Alessandra Crosato[b,c]

[a]Punjab Irrigation Department, Punjab, Pakistan; [b]Department of Water Resources and Ecosystems, IHE Delft Institute for Water Education, Delft, the Netherlands; [c]Department of Hydraulic Engineering, Faculty of Civil Engineering and Geosciences, Delft University of Technology, Delft, the Netherlands

ABSTRACT

In large rivers, most bridge crossings locally reduce the transverse floodplain width. This leads to adverse hydro-morphological effects, such as river bed and bank erosion, as well as increased upstream flood levels. In this study, we used a 2D morphodynamic model developed in Delft 3D to investigate the hydro-morphological impact of bridge span. The tool was applied to the Talibwala Bridge across the Chenab River in Pakistan. Our findings indicate that not only the length but also the location of the bridge span across the floodplain and bridge orientation influence the river hydro-morphodynamics. Smaller bridge spans exert more pronounced impacts, particularly during high flood events. We highlight that bridge span enlargement can serve as an effective intervention to reduce the adverse effects of existing bridges. These results emphasize the importance of considering the morphological river response during the design phase of bridges and of using morphodynamic instead of hydrodynamic models for flood level assessments.

ARTICLE HISTORY
Received 22 March 2024
Accepted 26 September 2024

KEYWORDS
Bridge crossing; Chenab River; Talibwala Bridge; Delft3D; bridge span

Introduction

Bridges are a vital component of modern transportation infrastructure, allowing people and goods to cross over rivers and other water bodies. However, their construction can also have significant impacts on the hydrodynamics and morphology of the rivers they cross, as for instance the increase in flood levels and the lateral shifting of the river channel upstream and downstream (Ali et al. 2021). This is particularly true for bridges crossing large braided and anabranched rivers since their span is mostly limited to the main channel. The closure of part of the floodplain at the crossing reduces the water conveyance during high flows and creates backwater effects upstream (Laursen 1970; Villada Arroyave and Crosato 2010). In addition, the flow concentration in a narrower area can cause bed and bank erosion. For instance, bank erosion increased after the construction of the Jamuna Bridge in Bangladesh (Bhuiyan et al. 2010) and of the Odlabari Bridge across the Chel River in India (Biswas and Banerjee 2018). These impacts can have negative consequences for the nearby human settlements and the fertile land adjacent to the river. One such example is the Dharala Bridge on the Dharala River in Bangladesh, where the extent of river bank erosion has become alarming for the adjacent community (Uddin et al. 2022). Yet, the causes of bridge-originated river bank erosion are not well understood (Hager and Unger 2010). Bridges often cause the formation of bars that divert the flow towards the bank, and this may happen also far upstream and downstream (Crosato and Mosselman 2020). This means that it is still difficult to design low-impacting bridges and plan efficient mitigation measures.

Remote sensing techniques have been employed in several studies (Alam et al. 2007; Islam 2013; Biswas et al. 2015; Oo et al. 2019; Uddin et al. 2022) in order to assess the hydro-morphological impacts of bridge construction on rivers. Methods based on data analysis are essential to identify and quantify the morphological effects of existing settings but do not allow assessing what would be the effects of other settings, with different bridge orientation, span and location across the river, including its floodplain. Numerical models provide the opportunity to analyse wider potential conditions and in combination with GIS, they can offer reliable results (Dysarz et al. 2023). In the numerical

CONTACT Muhammad Rizwan Akram rizwanakram3811@gmail.com Hayatabad Street No 1 House No 1 Chichawatni District Sahiwal, 57200, Pakistan

modelling domain, the focus so far has been the analysis and prediction of the morphological effects at the local spatial scale, as for instance the scouring around bridge piers (Mahmud et al. 2020). About larger spatial and temporal scales, only a few studies have been carried out. With a two-dimensional (2D) morphodynamic model, Azhar (2018) studied the development of bars caused by a bridge pier, either upstream or downstream. Abdou et al. (2021) analysed the effects of bridge span on bar formation at the new equilibrium river morphology but did not consider the effects of bridge-originated bars on bank erosion and channel shifting. By simulating the changes in river cross-section that occur during floods, a morphodynamic model would also allow for more realistic estimates of water levels during flood events compared to any hydrodynamic models based on fixed cross-sections, especially for rivers with relatively high mobile beds (Lee et al. 2006; Costabile et al. 2014; Ogras and Onen 2020; Crosato et al. 2022).

This work investigates the morphodynamic effects of a bridge across a vast river at a large scale, focusing on backwater effects, bar formation and river bank erosion. For the first time, the effects of several bridge designs, including a case with a different bridge alignment, are compared. The tool of investigation is made of two two-dimensional (2D) models developed in Delft3D: a fixed-bed hydrodynamic model and a mobile-bed morphodynamic model. Covering a longer river reach, the hydrodynamic model provides the boundary conditions for the more detailed morphodynamic model. To have a realistic numerical tool that can reproduce the effects of several bridge configurations, the set-up is based on a real case. The recently constructed Talibwala Bridge, crossing the Chenab River in the Punjab Province of Pakistan 65 km downstream of the Qadirabad Barrage, is chosen as the base-case scenario. Chohan et al. (2022) have shown that during high flows ponding occurs due to the construction of this bridge, which makes it an ideal case for the study. Moreover, significant bank erosion has occurred in the 6 km downstream and 6 km upstream of the structure. The choice of using this bridge as base-case lies also in the availability of data, such as water level and discharge time series, cross-sections and historical channel alignments, which has allowed for model calibration and validation. The simulation of several scenarios differing in bridge span and location across the river floodplain has permitted the comparison of the effects of various bridge configurations and identifying possible mitigation measures.

Study area

The Chenab River originates from the Indian Himalayas. It is called Chandra-Bhaga before entering Pakistan, where it meets the Jammu Tawi River and eventually joins the Indus (Ali et al. 2021). Annual monsoon-season flooding, resulting from heavy rainfall and northern Indian ice melt, strongly increases its water and sediment discharges (Chohan et al. 2022).

The region downstream of the Qadirabad Barrage, including the Talibwala Bridge area (study site), requires frequent flood management (Ashraf and Shakir 2018). Further downstream lies the Trimmu Barrage, constructed in 1939. The discharge of the river in the reach between the two barrages ranges between 4 m^3/s (lowest measured value) and 26,855 m^3/s, maximum value, measured on 11th September 1992 (Flood Forecasting Division 2023). The second peak discharge is 24,100 m^3/s, measured on 24 August 1996 and the third one is 21,917 m^3/s, measured on 07 September 2014. Using the Gumbel flood frequency analysis (Gumbel 1941) based on the available discharge data (the short period 1970–2021), these discharges are associated to return periods of 58, 35 and 23 years, respectively.

In the area around the Talibwala Bridge, the main river channel has an average width of about 2,000 m and its bed is made of sand, whereas the soil of the floodplains is made of fine sediment NESPAK (2010). The longitudinal bed slope is 0.32 m/km. The floodplain topography is characterized by higher elevation along the right bank of the river.

The Talibwala Bridge was initially constructed as a single carriage way in 1990 to connect the National Highway having an angle of 20 degrees with the river channel alignment. An extension with the addition of another dual carriage way (21.4 m wide) was built in 1997 with 34 spans of 26 m each. The super-structure consists of precast, pre-stressed girders with cast-in-place deck slab. The sub-structure consists of 2.0 m diameter bored cast-in-place piles (ENGINEERS 2021). Upstream of the bridge, for a length of 1,200 m, guide bunds on both sides of the river gradually reduce the river width to 905 m (Siddiqui et al. 2018; Ali et al. 2021) (Figure 1), which becomes 905 m at the bridge crossing. Moreover, during the building of the additional carriage way, construction debris was dumped on the river bed inside and around the three spans of the bridge furthest to the left. At present, the main channel is laterally shifting at outer bend locations, both upstream and downstream, as shown in Figure 1, and the dumped

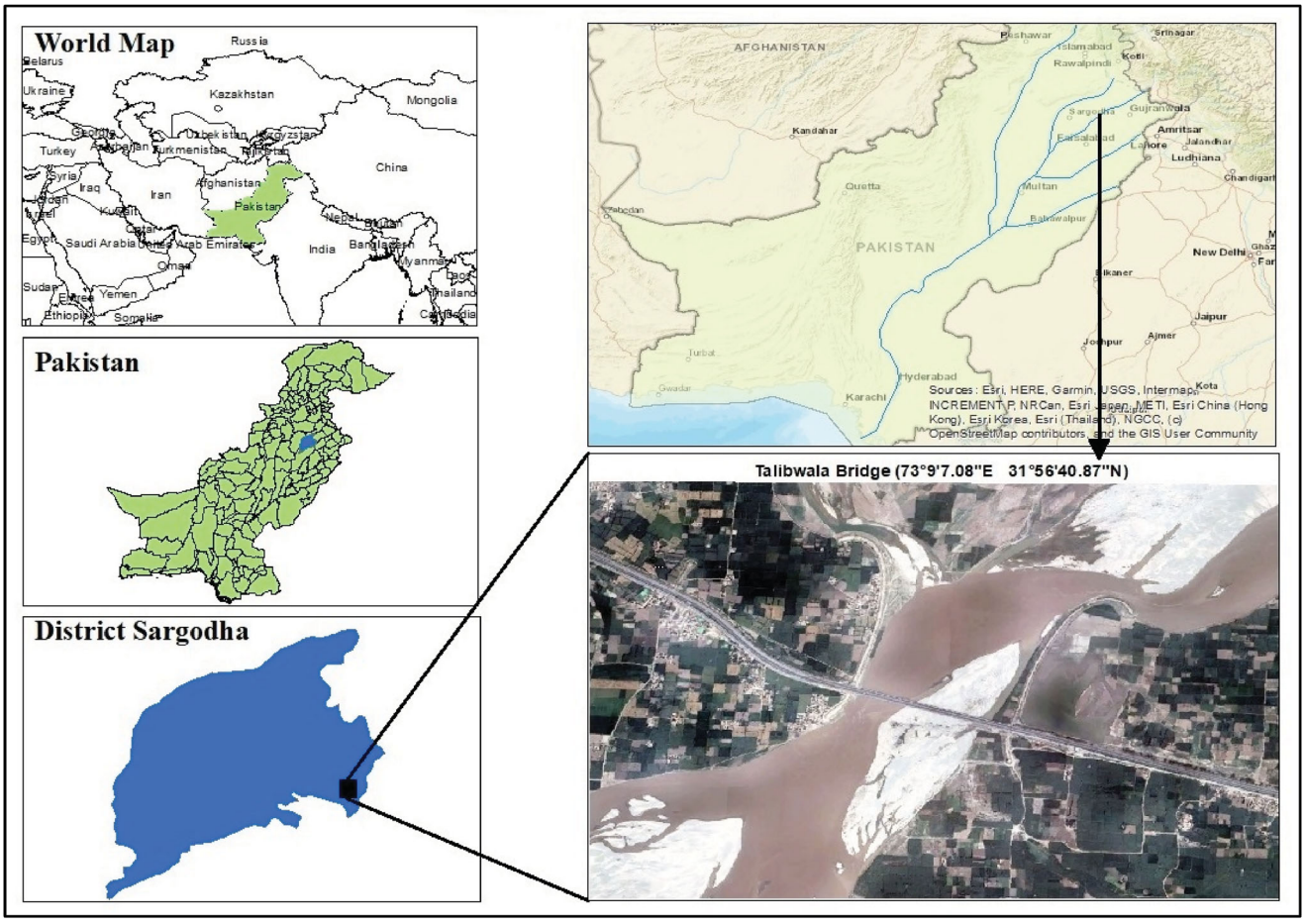

Figure 1. Study area location (Source: Google Earth).

debris is believed to be the main cause of this shifting. Bank erosion occurs mainly in the form of progressive mass failure. The growth of vast bars near the structure has invited the local people to utilize bar tops for agricultural purposes (Rasool et al. 2022), increasing the value of the land in the vicinity of the bridge. No bridges are present upstream of the Talibwala Bridge until the Qadirabad Barrage.

Methodology

The numerical tool was constructed using the open-source Delft3D-V4 software, which can be downloaded from https://oss.deltares.nl/web/delft3d/get-started. Delft3D models have been already successfully used to study the morphological changes of braided rivers (e.g. Singh et al. 2017; Hu et al. 2023) and proved to be computationally efficient (Parsapour-Moghaddam et al. 2023), which justifies the choice of the software.

We built two distinct models: (1) a fixed-bed hydrodynamic model, covering the 227 km long river reach between the two barrages of Qadirabad and Trimmu and (2) a mobile-bed morphodynamic model with higher resolution, covering a shorter reach around the Talibwala Bridge. The morphodynamic model was constructed by adapting and cutting the hydrodynamic model, which was in fact created to generate its boundary conditions.

Available data

The Punjab Irrigation Department of the Ministry of Irrigation Punjab, Pakistan (Department 2023) provided the daily discharge and water level time series covering the period January 2010–December 2021 at three gauge-stations: the Qadirabad Barrage (65 km upstream of the Talibwala Bridge), the Chiniot Bridge (32 km downstream of the Talibwala Bridge) and at the Trimmu Barrage (162 km downstream of the Talibwala Bridge). The discharge time series measured at the Qadirabad Barrage had several missing values, especially in the dry periods (periods that are less important for this study focusing on flood levels and morphological changes). After having interpolated the missing values and removed the outliers, data validation was

performed by cross-checking with the values of the discharges measured at the Chiniot Bridge. As there is no water withdrawal in the river reach between the Qadirabad barrage and the Chiniot Bridge, there should be a good correlation between the values of discharge at these two successive stations, considering a certain time lag. To assess the correlation, we applied two statistical methods: correlation coefficient and regression analysis. The maximum value of the correlation coefficient (0.878) was obtained for a time lag of 36 h, which can be considered reasonably good. For the same time lag, the value of R-Squared resulted in 0.775. These results indicate that upstream and downstream data are consistent.

The Lahore River Survey Division of the Ministry of Irrigation Punjab, Pakistan, provided also the river cross-sections measured in 2010, covering the area from 65 km upstream to 162 km downstream of the Talibwala Bridge, and in 2018, covering only the area upstream of the Talibwala Bridge. The cross-sections of 2010 regard only the main river channel(s) (no floodplain elevations) and are very distant from each other, with the average distance between two successive cross-sections being of the order of 5 km.

NESPAK (2010) sampled the bed material in the 227 km long reach between the Qadirabad Barrage to the Trimmu Barrage and found that the median grain size ranges from 0.09 to 0.250 mm, with larger values in the upper part of the river. In the area around the Talibwala Bridge the sediment size ranges between 0.200 and 0.250 mm.

Hydrodynamic model

The hydrodynamic model domain covered a length of 227 km, from the Qadirabad Barrage to the Trimmu Barrage, for a width of 24 km to include the entire floodplain area. The discharge time series measured at the Qadirabad Barrage during the flow season of the year 2014 constituted the upstream boundary condition, and the water-level time series measured at the Trimmu Barrage during the same period the downstream boundary condition.

The land boundary map, defining the model domain, was developed using GIS and SRTM satellite images of the year 2000, having a resolution of 30 m (downloaded from the website of U.S. Geological Survey; https://earthexplorer.usgs.gov/).

The bed topography of the main river channel(s) was set up using the cross-sections measured in 2010, integrated by GIS and SRTM data were necessary, whereas the floodplain elevation was derived from the 2018 survey.

The structured curvilinear grid, following the contour of the main river channel, was imposed cell sizes between 146 and 455 m in the longitudinal direction, and between 24 and 854 m in the transverse direction (Figure 2), with the largest grid cells belonging to the floodplain area. The grid size was chosen based on the resolution required for a satisfactory water level assessment, and on computational efficiency, as the hydrodynamic model was very lengthy (computational time of the order of two weeks).

Due to uncertainty in bed roughness (Dysarz et al. 2023), hydrodynamic model calibration aimed at optimizing the value of Manning's coefficient. For this, the water levels computed for the flood season of the year 2014 at the location of the Chiniot Bridge (intermediate location) were compared to the ones measured at the corresponding gauge station. Hydrodynamic model validation was subsequently carried out by comparing the water levels computed by the calibrated model in the period 2010–2013 at the same gauge station.

Theoretically, if we consider the smallest cell size of the model, the time step should be less than 41 s. However, due to computational time constraints and considering the average cell size of 307 m, we imposed a time step of 60 s (Courant numbers smaller than 0.7), since it did not produce any instability and the solution always converged in preliminary runs.

Morphodynamic model

The morphodynamic model was constructed from the hydrodynamic model. The domain was cut and the grid was refined to keep a balance between the computational time and the accuracy of the results. To reduce the effects of errors at the boundaries (values derived from the hydrodynamic model), the location of the downstream boundary was established considering the length of the backwater caused by the Chiniot Bridge, and the location of the upstream boundary considering the length of the backwater caused by the Talibwala Bridge itself. Backwater lengths were roughly derived for the annual peak discharges during the study period (2010–2017) by using the simple formula (four times the analytical half-length by Bélanger 1841):

$$L = h/s \tag{1}$$

where L is the backwater length (m), h is the reach-averaged water depth at the annual peak discharge (m) and s is the longitudinal bed slope of the considered river reach (-).

The boundaries were established at the backwater half-length, being 1/4 of L, i.e. 17 km upstream and 17 km downstream of the Talibwala Bridge. Within the

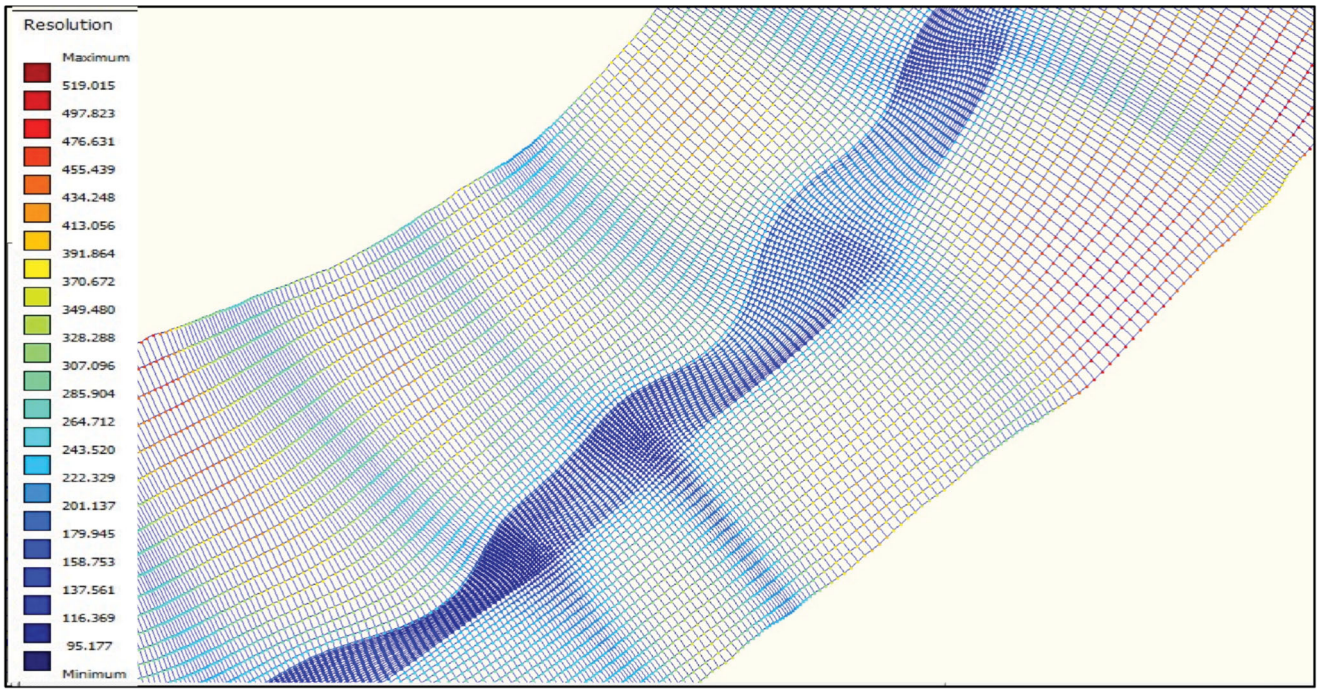

Figure 2. Part of the hydrodynamic model grid.

model domain, the study area extended from 6 km upstream to 6 km downstream of the bridge, where the morphological effects of the bridge were mostly observed.

The size of the structured curvilinear grid cells varied in longitudinal direction from 52 m to 227 m and in transverse direction from 36 m to 207 m, with the largest cell sizes belonging to the floodplain area. In the focus area (6 km upstream and 6 km downstream of the bridge), the cell size varied from 76 m to 97 m and from 72 to 114 m, respectively. The morphodynamic model was run with the same time step as the hydrodynamic model (60 s), since in preliminary runs also this model never produced instability and the solution always converged.

Considering that the measurements did not show any notable changes in discharge in the reach between the Qadirabad Barrage and the Talibwala Bridge, the discharge time series imposed at the upstream boundary coincided with the (corrected) time series measured at the Qadirabad Barrage. The water levels time series at the downstream boundary were extracted from the hydrodynamic model.

The sediment input from upstream and the sediment leaving the model domain (upstream and downstream boundary condition for sediment, respectively) were computed by using the formula of Engelund and Hansen (1967), designed for sand-bed rivers, which was applied also to compute the sediment transport capacity in the entire model domain. Based on NESPAK (2010) and assuming uniform sediment (medium sand), we imposed a median grain size of 250 µm. Flokstra and Koch's (1981) formulation was used to correct the sediment transport direction by considering the effects of transverse bed slope.

Bank erosion was imposed as bed erosion in the dry cells following the channel margin. For this, the value of a calibration coefficient indicates the percentage of bed lowering that is imposed on those dry cells that are adjacent to eroding wet cells (Lesser et al. 2004; Deltares 2023). This allows some dry cells to become wet and participate in the morphological development as part of the river channel.

Model calibration and validation were based on qualitative and, where possible, quantitative comparisons between model predictions and observed morphological changes in the periods 01 January 2010–31 December 2017 and 01 January 2018–31 December 2021, respectively. These changes included river bank shifting, bar size growth and planimetric changes of the river derived from remote sensing and in situ surveys.

The coefficients that were tuned to calibrate the morphodynamic model are: A_{shld}, coefficient weighing the transverse bed slope effect; *ThetSD*, factor for the erosion of the dry cells adjacent to the wet river margin; and E_{spir}, coefficient weighing the spiral flow intensity. In addition, we also calibrated the value of the eddy diffusivity. The calibration process involved systematically adjusting the value of each coefficient while keeping the others constant. A total of six simulations were run

Table 1. Simulation runs for model calibration.

Model Run	ThetSD (-)	A_{shld}(-)	Eddy Diffusivity (m^2/s)	E_{spir}(-)
CalRun 01	0.4	1.5	10	1
CalRun 02	0.5	1.5	10	1
CalRun 03	0.5	0.7	10	1
CalRun 04	0.5	0.7	5	1
CalRun 05	0.9	0.7	5	1
CalRun 06	0.5	0.7	10	3

for the period of 8 years starting from 01 January 2010 and ending on 31 December 2017 (Table 1). The runs started with the same bed topography as in the hydrodynamic model (based on the surveys made in 2010) in which dry cells were introduced to represent the guide bunds and the road crossing across the flood plain (initial condition).

The calibration was based on the best match with the river survey carried out by the Punjab Irrigation Department in Jan. 2018 at a distance 2,514 m, 3,778 m, 5,088 m and 5,488 m upstream of the bridge and with the planimetric changes derived from the analysis of the remote sensing images acquired from the USGS website at low flow conditions (https://earthexplorer.usgs.gov). For the calibration of the bank erosion coefficient, the results of the model were compared with the bank shifting observed in the period Jan. 2010 – Dec. 2017.

The calibrated model was run for the period 01 January 2018–31 December 2021 in order to validate the results. For this, we used the observed bank shifting. Due to a lack of cross-sectional surveys after Jan. 2018, the validation of the model with respect to its ability to (qualitatively) reproduce the changes in bed topography was based on the comparison between the simulated sand bar growth and the bar growth that has actually occurred, which can be detected from the remote sensing images that were taken at low flows.

Remote sensing

Due to limited ground survey data for morphodynamic model calibration and validation, remote sensing data analysis was performed to investigate the historical changes in the river during the study period. Landsat 8 images having a resolution of 30 m were downloaded from the website of the United States Geological Survey (USGS) taken during low flow. As the built-up area is not significant at the location that could affect the delineation, these images were downloaded within Band 5 (NIR) and Band 3 (Green) to differentiate the water from the river bank using the Normalized Difference Water Index (McFeeters 2013). The images were processed for classification in QGIS based on the threshold value of NDWI to detect water. Shape files were created to draw polygons representing the river channel boundary, bars, and centrelines for each image separately. These polygons were overlapped at the same scale to quantify changes, such as bank shifting and bar formation.

Study scenarios

Seven scenarios were selected for the purpose of the study.

The actual bridge configuration including the dumped debris served as the base-case, but for sake of generalization, the bridge was made perpendicular to the river channel (in reality the Talibwala Bridge is not exactly perpendicular, since it forms an angle of 20 degrees to the river channel alignment).

In the second scenario, the debris dumped on the left side of the Talibwala Bridge is removed. This scenario has been defined to test the hypothesis that this material is the cause of the observed local bar growth and consequent erosion of the opposite river bank along the downstream right side of the river.

The third scenario has the bridge span width equal to the average width of the main river channel in the area. The underlying assumption is that this bridge span would suffice to cease the shifting of the channel and lower the flood water level at the upstream side.

Scenarios four and five have equal bridge spans, but with extensions at opposite sides of the floodplain, which differ in surface elevation. These two scenarios are built to assess the optimal bridge span extension while testing the assumption that including the lower elevation floodplain would be more effective in reducing the hydro-morphological changes than including the higher floodplain also on the long term.

Scenarios number six and seven present further widening of the bridge span, but in a symmetric way, with the aim to determine the nature of the relation between hydro-morphological changes and the bridge span.

For the sake of simplicity, the model does not include the energy losses due to the presence of bridge piles. Due to the coarse grid of the model, piles would be sub-grid structures and their presence could only be considered in terms of local energy loss through an increase of the roughness coefficient. The presence of piles and their number depend on how the bridge is constructed and so does the local energy loss. This means that the value to be attributed to the Manning coefficient at the bridge crossing would be different from case by case. It is important to consider that neglecting the local energy losses would imply the underestimation of water levels and local bed erosion. This means that the results of

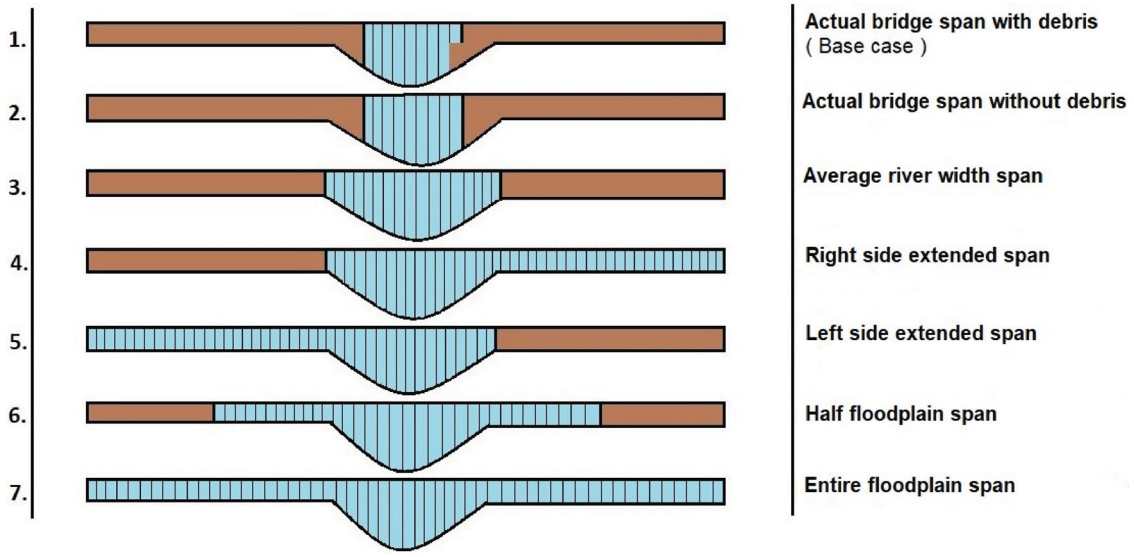

Figure 3. Configuration of scenarios for the model runs.

Table 2. Bridge configuration scenarios and their span width.

Scenario	Bridge span (m)
Actual bridge span with debris (Base-case)	905 m
Actual bridge span without debris	905 m
Average river width span	2,135 m
Right side extended-span (from left abutment of bridge to right flood embankment)	5,450 m
Left side extended-span (from right abutment of bridge to left flood embankment)	5,450 m
Half floodplain span (between the flood embankments)	5,000 m
Entire floodplain span (between the flood embankments)	10,000 m

the model cannot be used to study absolute values but to compare the effects of different configurations. The bridge span for each scenario is indicated in Table 2 and the configurations of scenarios are shown in Figure 3.

The simulation period covers 8 years (1st Jan. 2010 to 31st Dec. 2017). The comparison of high flow levels is carried out for the discharge of 21,917 m^3/s that was measured on 07 September 2014, having an expected return time of 23 years. The comparison of sediment transport rates is carried out for the same discharge. However, the comparisons of bed level changes in the vicinity of the bridge, of cumulative sediment transport at the cross-sections upstream and downstream of the bridge and of the cross-sectional changes downstream of the bridge are based on the results of the model at the end of the simulation period.

Results

Data processing

The result of data processing regarding the discharges measured at the Qadirabad Barrage is the daily time series of Figure 4, used as the upstream boundary condition. The comparison with the discharge time series of the Chiniot Bridge produced a correlation coefficient equal to 0.878 and the regression analysis resulted in the R-squared value of 0.775.

The cross-analysis of the discharge time series showed that in the 97 km that separate the Qadirabad Barrage and the Chiniot Bridge, the Chenab River loses 17.8% of its discharge on average. Most losses (22.4%) occur during the dry season, which is in winter, when the flow is at its minimum, mainly due to seepage. Agriculture withdrawal occurs only upstream of the Qadirabad Barrage (https://irrigation.punjab.gov.pk/dynamic-line-diagram).

The losses have been calculated in this study by using the discharge time series at the two stations (one upstream and the other downstream of the study area). The average difference of discharges in terms of percentage has been used to establish these statistics.

The analysis of historical satellite imagery from 2010 to 2021 revealed the planimetric changes of the Chenab River in the study area. These are presented in Figure 5 with different colour lines. Bank erosion is visible along the outer bends, both upstream (left bank) and downstream (right bank) of the bridge. Between January 2010 and December 2017, the maximum bank line shift was 250 m upstream and 180 m downstream; from Jan. 2018 to Dec. 2021, 350 and 420 m, respectively.

The analysis of historical satellite images taken during low flows (Figure 6) also allowed the delineating also the horizontal topographic changes of the river channel bed. Between 2010 and 2021 bars have grown in size, as for instance the forced bar at the left side of the bridge. The central bar just upstream of the bridge

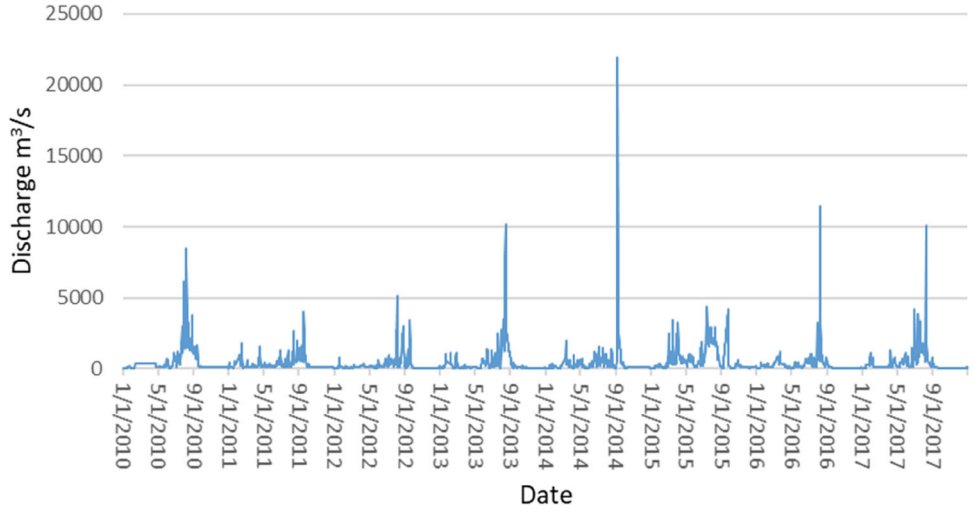

Figure 4. Processed Discharge Time Series at the Qadirabad Barrage (m^3/s).

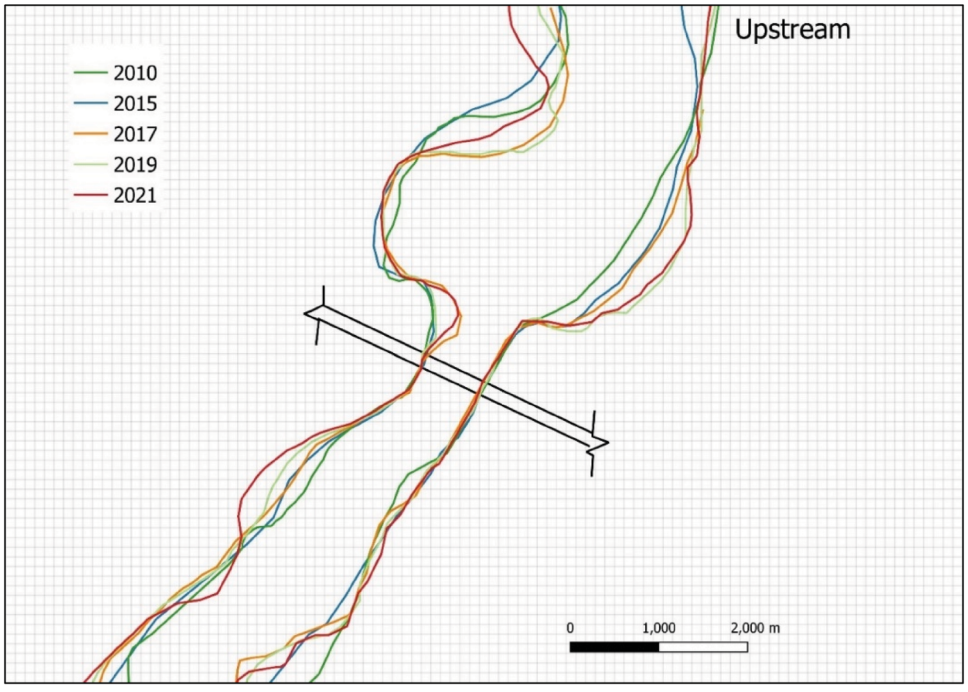

Figure 5. Alignments of main channel banks in the period 2010–2021 at the location of the Talibwala bridge.

increased in transverse direction by 450 m from 2010 to 2017 and by 575 m from 2017 to 2021. Furthermore, also the channel sinuosity increased. Upstream of the bridge, the sinuosity index, the ratio between the length of the channel along the thalweg and the length of the valley along its axis (Mueller 1968), rose from 1.16 to 1.45 between 2010 and 2021. Upstream of the bridge, the bar area grew from 5.9 km^2 in 2010 to 18.6 km^2 in 2021. Instead, the bar area decreased downstream of the bridge from 11.07 km^2 to 5.24 km^2. The bar at the bridge location started emerging in 2015 and its surface area increased from 0.16 km^2 to 0.81 km^2 in 2021. The bar just upstream of the bridge transformed from elongated to rounded, since its length-to-width ratio reduced from 3.15 in 2010 to 0.85.

Hydrodynamic model calibration and validation

Hydrodynamic model calibration was obtained through the comparison between computed and measured water levels at the Chiniot Bridge in the period 10 February 2014 to 08 October 2014. The best results were achieved for Manning's roughness coefficient of 0.045 $m^{-1/3}s$, imposed to the entire model domain. The

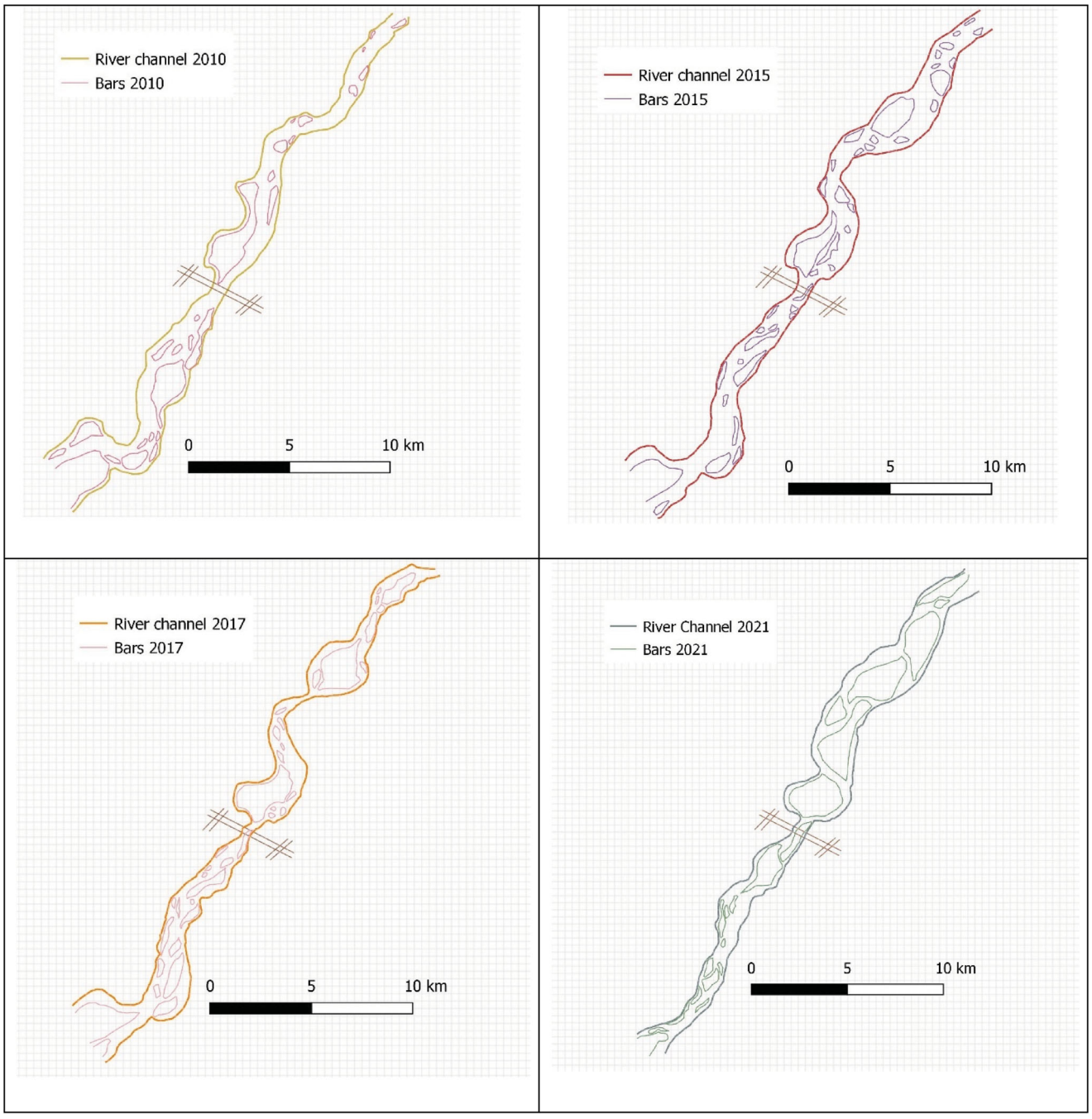

Figure 6. Emerging bars and main channels margins in 2010, 2015, 2017 and 2021 at low water conditions in the study area.

results of hydrodynamic model calibration are shown in Figure 7.

Model validation was based on the comparison between computed and measured water levels at the Chiniot Bridge in the period 2010–2013. The results are shown in Figure 8. At low-flow conditions, the model overestimates the water levels by about half a meter. The reason is that the deepest parts of the river channel that convey the flow at the lowest discharges are too narrow compared to the grid cell sizes and are therefore not represented in the model. At the same time, however, the model underestimates the peak water levels by also about half a meter. There are multiple reasons for this underestimation: the floodplain roughness is in reality higher than the roughness imposed on the model, which is the same everywhere; the hydrodynamic model does not incorporate all the obstructions, such as embankments, settlements and bridges that reduce the floodplain surface area. However, considering the scope of the work, i.e. the comparison between scenarios, it was considered not necessary to further refine the model.

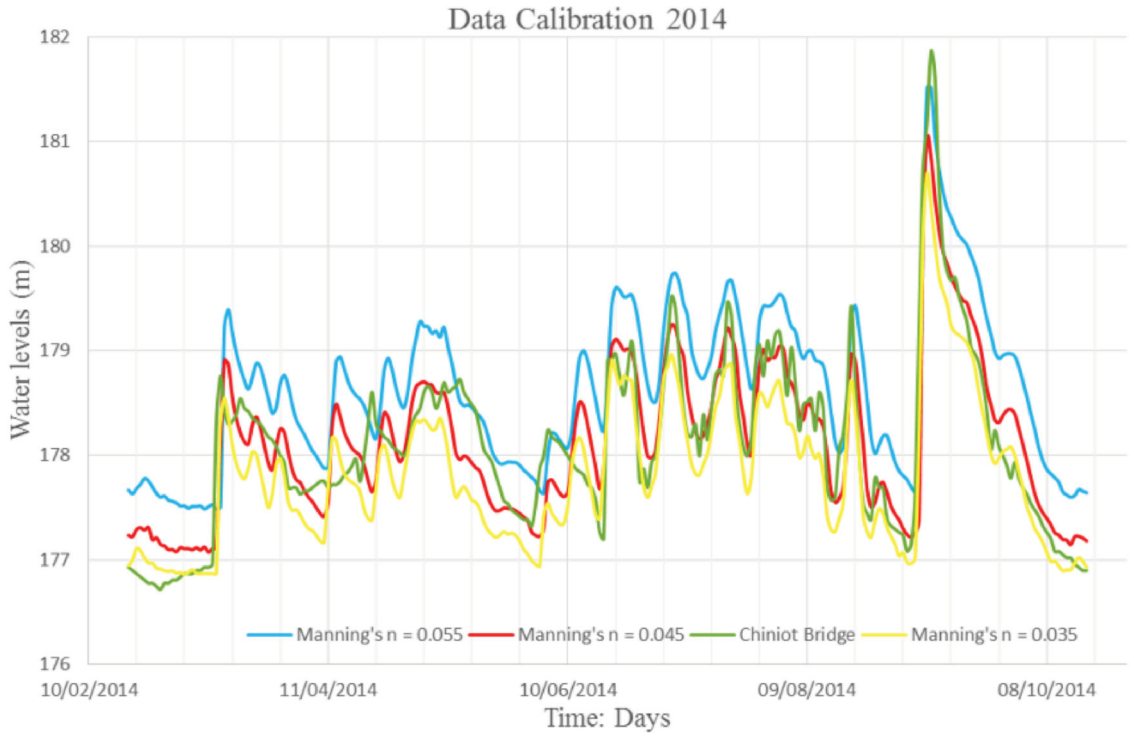

Figure 7. Water levels at the Chiniot Bridge. Results for different values of Manning's roughness coefficient (0.035, 0.045, 0.055 $m^{-1/3}s$). The measured water levels are iven in green.

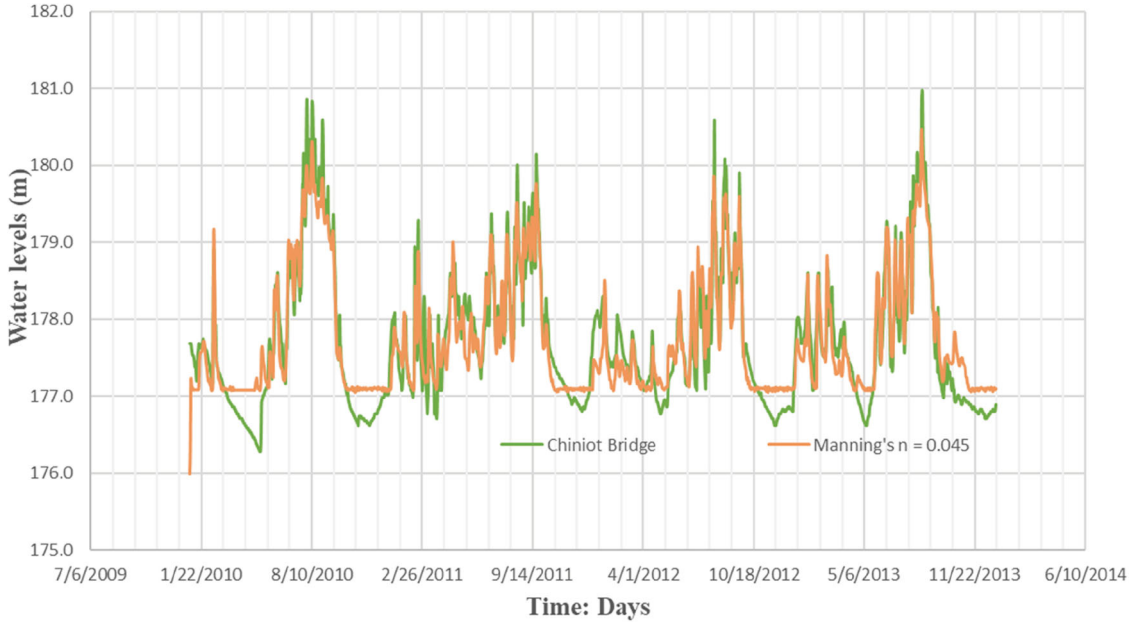

Figure 8. Water levels at the Chiniot Bridge. Results of the validation run adopting the calibrated value of Manning's roughness coefficient (0.045 $m^{-1/3}s$). The computed water levels are in presented in orange, the measured ones in green.

Morphodynamic model calibration and validation

The calibration of the morphodynamic model was based on the ability of the model to predict the bank retreat that occurred in the period January 2010–31 December 2017 at a distance of 1,360, 1,520 and 1,660 m downstream of the Talibwala Bridge. The modelled average bank retreat was 130 m, with a maximum of 200 m at the most downstream location. This result is comparable to the one derived from the satellite images, with a maximum bank retreat of about 180 m. As the satellite images have a resolution of 30 m, the

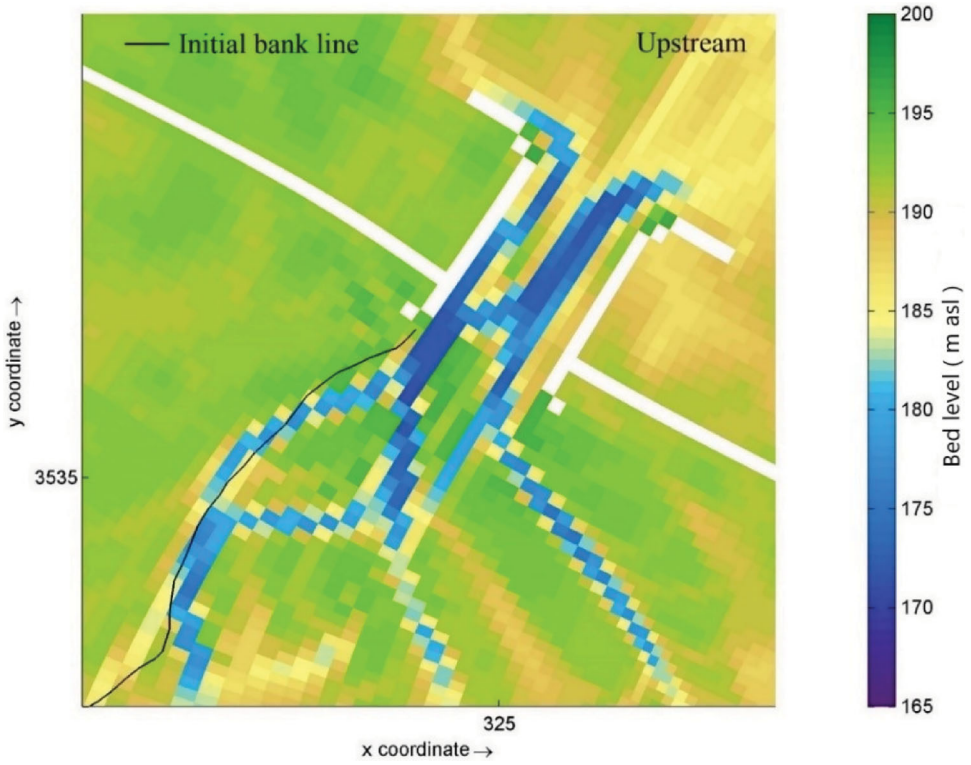

Figure 9. Results of morphodynamic model calibration: computed bed level in 31 December 2017. The road crossing the Chenab River by means of the Talibwala Bridge and the guide bunds are indicated in white. The thin black line corresponds to the channel margin in 2010.

estimate involves uncertainty (+/− 30 m), but despite this uncertainty, the qualitative comparison shows good agreement. The bed topography of 31st Dec 2017 computed with the calibrated model is shown in Figure 9. The modelled bank alignment follows the one derived from the satellite image of 24th August 2017 rather well. However, the model seems to overpredict the size of a creek crossing the left floodplain. This creek was also present in the satellite image, but it is not included in the pictures showing the margins of the main river channel (Figures 5 and 6). The calibrated values of the coefficients listed in Table 1 are: $A_{shld} = 0.7$, *ThetSD*, $= 0.5$, E_{spir}, $= 1$, eddy diffusivity $= 10\,m^2/s$.

Figure 10 shows that the computed cross-sections have a good match with the observed ones in terms of number of channels, bars and thalweg line.

The validation of the calibrated model, specifically on its ability to simulate bank erosion, was based on the comparison between computed and observed bank shifting in the period January 2018–December 2021. The latter indicates good agreement between model and observations, presenting the same trend at the same locations (Figure 11).

At the end of the validation period, the computed river channel reveals the persistence of bank erosion, shown as cumulative bed erosion near the channel margin, along the outer bends upstream and downstream of the bridge. These locations are indicated in Figure 12 with red circles. Downstream of the bridge, cumulative deposition (shown in green to dark red) reflects the growth of an existing vast bar towards the right side of the river. This bar extension gradually pushed the flow to the right, enhancing opposite bank erosion. Model results show also the growth of a bar just upstream of the bridge, near the start of the guide bund, at the left side of the river. These simulated developments agree qualitatively with observations (Figure 6).

Scenarios

The longitudinal profiles of water levels computed with the morphodynamic model for the peak discharge of $21{,}917\,m^3/s$ are shown in Figure 13. Scenarios 1 and 2 (actual bridge span with and without debris) produce the highest water levels, with the maximum level being 2.4 m higher than the one obtained for scenario 7 (entire floodplain span scenario). This result shows also that the presence of the dumped debris has only negligible impact (< 0.02 m) on flood levels. For a bridge span equal to the average main channel width (scenario 3), the maximum water level increase with respect to

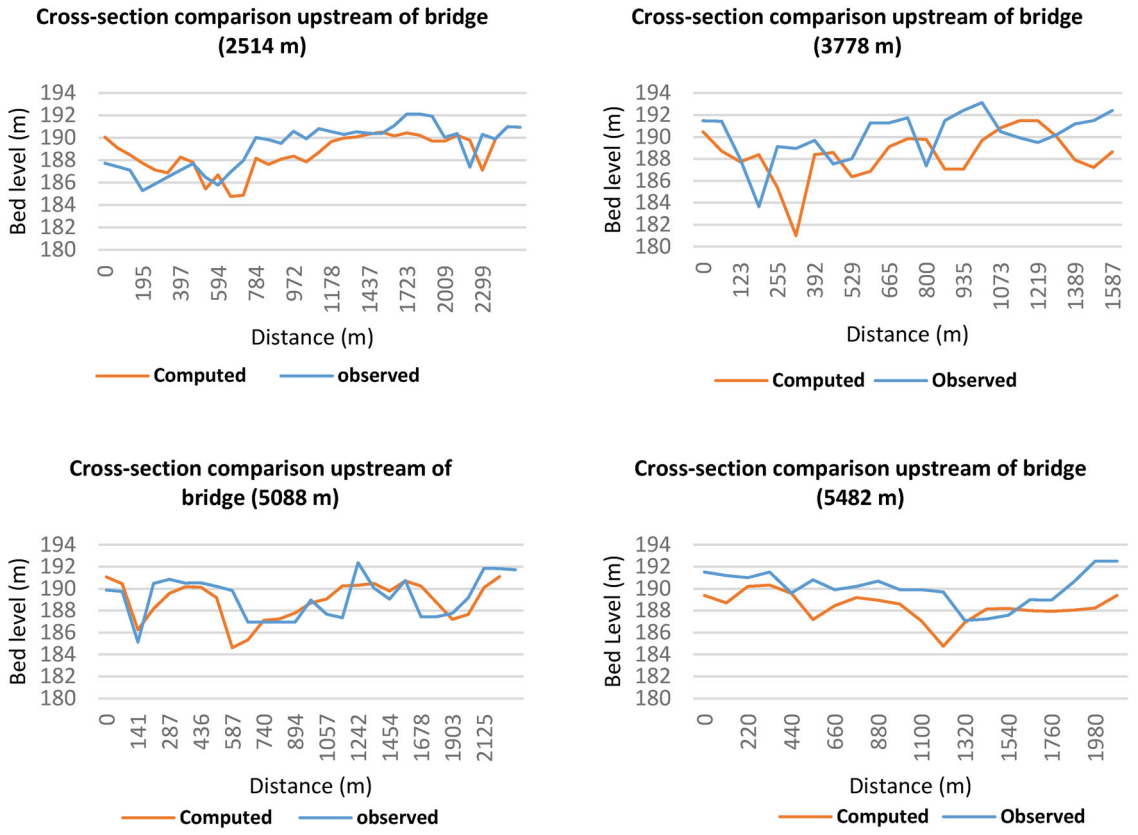

Figure 10. Results of morphodynamic model calibration: computed and observed cross-sections in Jan. 2018 (River Survey by the Division of the Ministry of Irrigation Punjab, Pakistan) at 2,514, 3,778, 5,088 m and 5,482 m upstream of the Talibwala Bridge.

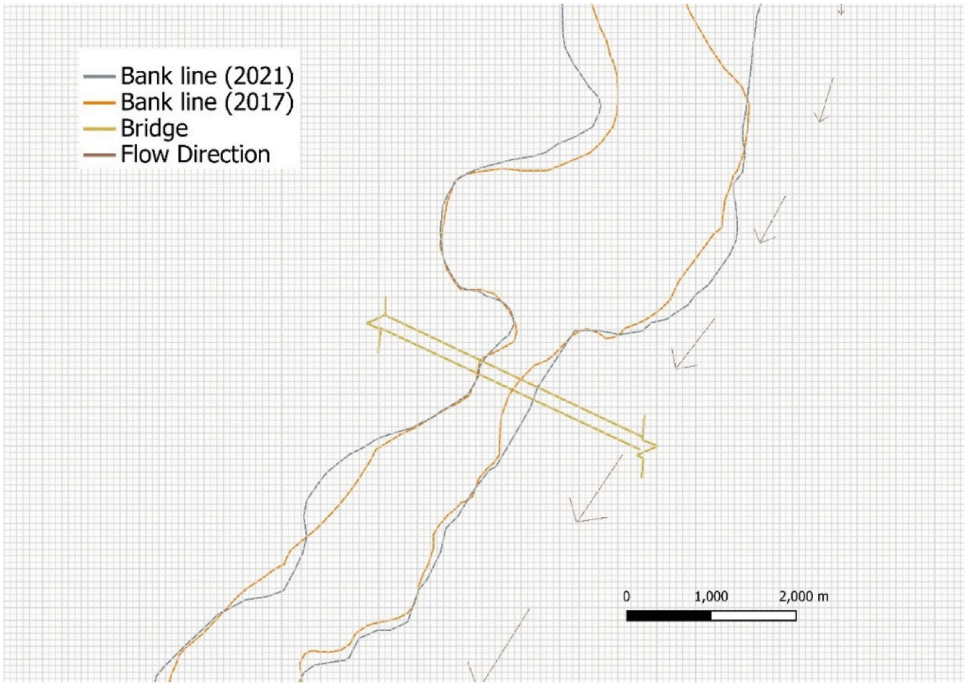

Figure 11. River bank lines derived from the satellite images of 24th Aug. 2017 and 19th Aug. 2021.

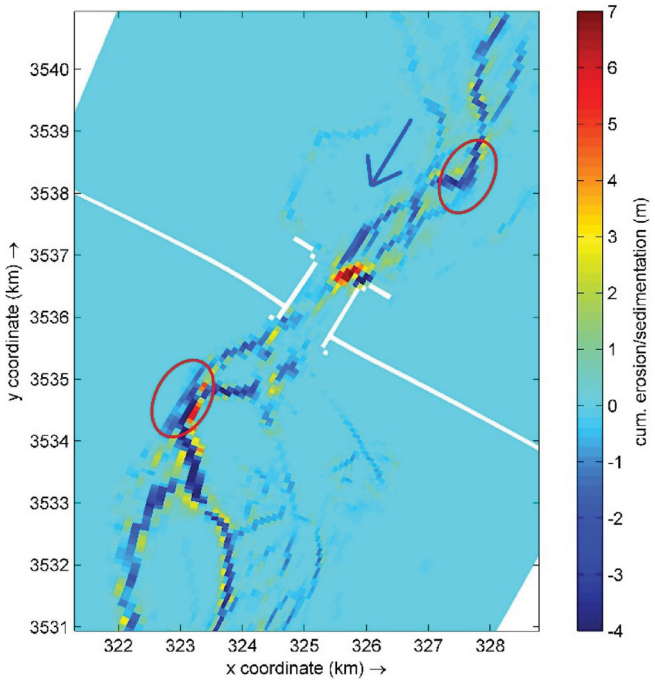

Figure 12. Results of morphodynamic model validation: cumulative bed erosion (negative values) and sedimentation (positive values) in the period 1st Jan. 2018–31st Dec. 2021. The road crossing the Chenab River built on embankments at the right and left sides of the Talibwala bridge and the guide bunds are indicated in white. The flow direction is indicated by a blue arrow. The circles indicate the location of the maximum bank retreat.

scenario 7 becomes 0.95 m. The difference in water level with the scenario with the span extended to the left-side (scenario 5) is small, but this difference becomes comparable to scenario 3 (0.75) m if the bridge span is extended to the right where the floodplain is higher (scenario 4). Approaching the bridge, the water level gradient increases reaching its maximum value just past the bridge and then decreases. The trend is similar for all scenarios, except for the entire floodplain span bridge (scenario 7) where the gradient is almost constant near the bridge. The water level gradient is the highest for the actual bridge span (scenarios 1 and 2). At distances over 3,000 m downstream from the bridge, the water levels and their gradients are similar for all scenarios. The downstream boundary condition is the water level time series computed by the complete hydrodynamic model 17 km downstream of the Talibwala Bridge and is the same for all scenarios. Being the half condition of the models 17 km (Equation 1), it is clear that the boundary condition influences the results in the study area, especially in its most downstream part. As a consequence, the results downstream of the bridge close to the boundary should be compared to derive only qualitative trends and not quantitative ones. It can be therefore observed that the influence of bridge span on water levels is limited to the first 2 km downstream, whereas the bridge span affects the water levels in the entire model domain upstream of the bridge, the backwater length L being in the order of 70 km (Equation 1).

The computed longitudinal profiles of cross-section averaged flow velocity are shown in Figure 14. The base-case (scenarios 1 and 2) presents the highest flow velocity near the bridge, ranging from 1.3 m/s to 3.5 m/s; the case with a bridge span covering the entire floodplain (scenario 7) is the lowest. At the same time, the base-case scenario produces the lowest flow velocity far upstream (approximately 0.5 m/s). This is because this scenario produces the highest rising of water level. Downstream of the bridge, all velocities converge to the value imposed by the boundary condition. The comparison between scenarios 4 and 5, with the bridge span extending either to the right or to the left, indicates that higher flow velocities can be expected for the former scenario. This is because the right side of the floodplain is higher, acting as a barrier against the flow in the transverse direction. The longitudinal velocity profile for the bridge span extending to the left (scenario 5) is comparable to the half floodplain span scenario (scenario 6). This is due to the lower floodplain elevation on the left side of the river, providing a wider space for the water to flow through.

The longitudinal profiles of sediment transport rate at the peak discharge of 21,917 m^3/s are shown in

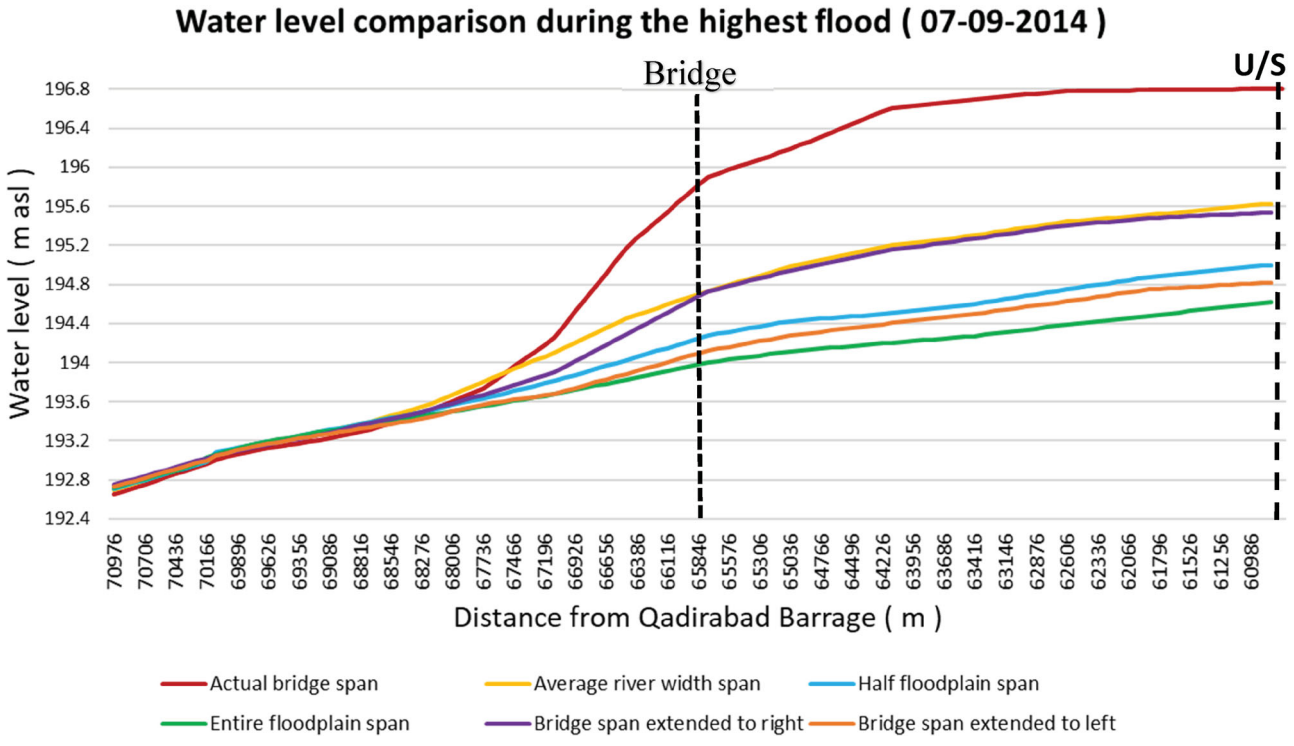

Figure 13. Longitudinal profiles of water levels were computed for the different scenarios at the peak discharge of 21,917 m^3/s measured on 07 September 2014. Due to negligible difference scenarios 1 and 2 are not distinguished.

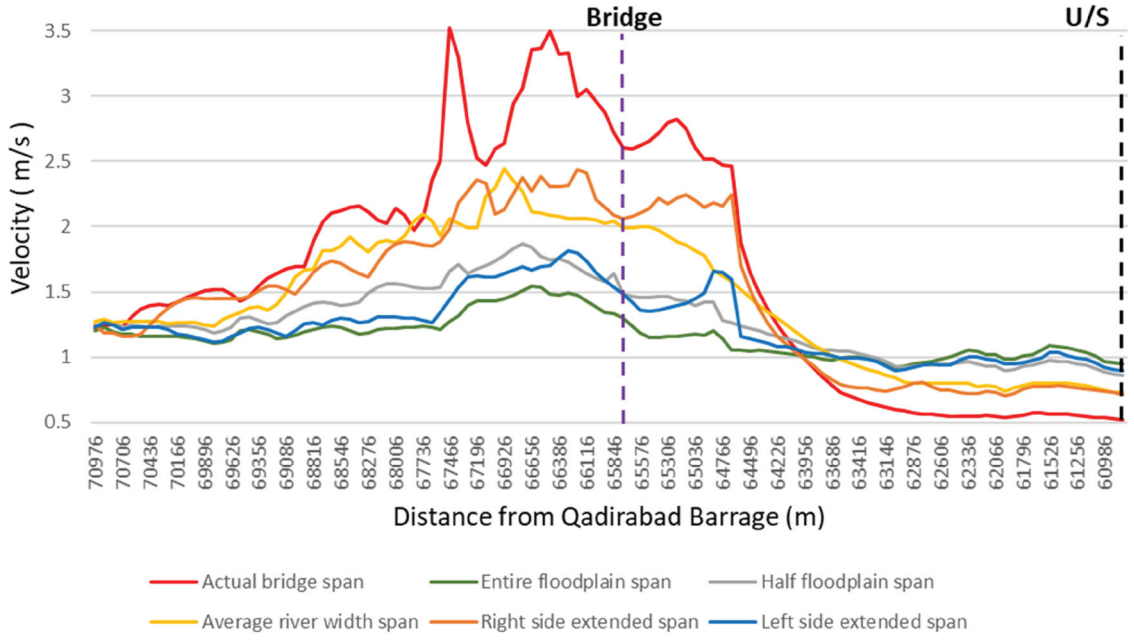

Figure 14. Longitudinal profiles of cross-section averaged flow velocity computed for the different scenarios at the peak discharge of 21,917 m^3/s measured on 07 September 2014. Due to negligible difference scenarios 1 and 2 cannot be distinguished.

Figure 15. Near the upstream boundary, the base-case (scenarios 1 and 2) presents the minimum sediment transport rate, which is consistent with the highest water level rise with the lowest flow velocities. On the other hand, the base-case produces the maximum sediment transport rate at the bridge location, due to the highest velocity. This means that the base-case scenario produces the maximum bed erosion rates during high flow conditions.

Table 3 lists the cumulative volumes of transported sediment at the end of the computation period (8 years, from 1st Jan. 2010 to 31st Dec. 2017) at two

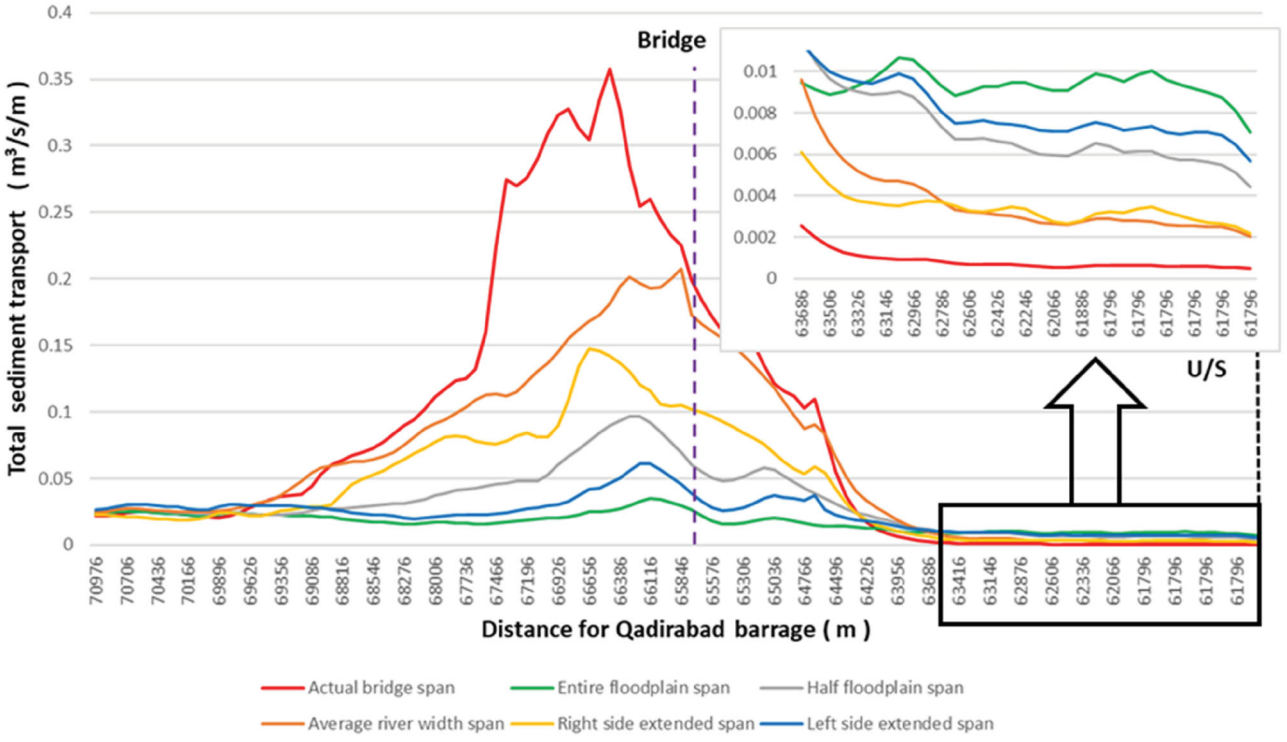

Figure 15. The longitudinal profile of sediment transport rate computed for the different scenarios at the peak discharge of 21,917 m^3/s, measured on 07 September 2014. Due to negligible difference scenarios 1 and 2 are not distinguished.

Table 3. Cumulative volumes of transported sediment at the end of the computation period (01 January 2010 to 31 December 2017) at indicated distances from the bridge.

Distance	Scenario 1	Scenario 2	Scenario 3	Scenario 4	Scenario 5	Scenario 6	Scenario 7
2,055 m Upstream (m^3)	1.0×10^6	1.0×10^6	1.144×10^6	1.102×10^6	1.14×10^6	1.16×10^6	1.16×10^6
1,590 m Downstream (m^3)	5.01×10^6	5.01×10^6	3.88×10^6	3.99×10^6	2.44×10^6	2.87×10^6	2.42×10^6

cross-sections. Two virtual cross-sections were put in the model, one 2,055 m upstream of the bridge and the other 1,590 m downstream, to check the sediment transport difference at the two locations. Scenario 5 (bridge extended over the lower left floodplain) and 7 (bridge over the entire floodplain) produce similar results, indicating that the higher floodplain acts as an obstacle to the flow in the transverse direction, which makes scenario 7 similar to scenario 5. The presence of the dumped material does not influence the sediment transport (compare scenarios 1 and 2). The increase in the volume of transported sediment from upstream to downstream of the bridge indicates bed erosion in the area between the two cross-sections. The lowest differences belong to scenarios 7 and 5, the highest to scenarios 1 and 2.

Figure 16 shows the longitudinal profiles of thalweg elevation at the end of the simulation period (1st Jan. 2010–31st Dec. 2017). Bed erosion appears concentrated in a 6 km long reach, starting approximately 2 km upstream and ending 4 km downstream of the bridge, with the highest values slightly downstream of the bridge. As expected, the base-case (scenarios 1 and 2) produces the highest bed erosion; followed by scenario 4, with the bridge span extended to the right. All the other scenarios present rather similar thalweg profiles, indicating similar bed erosion (scenarios 5–7), with scenario 6 presenting slightly more bed erosion in the area upstream of the bridge.

Figure 17 depicts the computed cross-sections at a distance of 1,486 m downstream of the bridge at the end of the computation period. All bridge configurations caused the river to shift towards the right. Scenario 4 (bridge span extended to the right) resulted in the least lateral shift, whereas the largest shift pertains to the actual bridge span (base-case, scenarios 1 and 2). Scenario 7 (bridge span over the entire floodplain) and scenario 5 (bridge span extending to the left side) produce similar results.

Discussion

The comparison between the flood levels obtained with the hydrodynamic model (fixed bed) and the

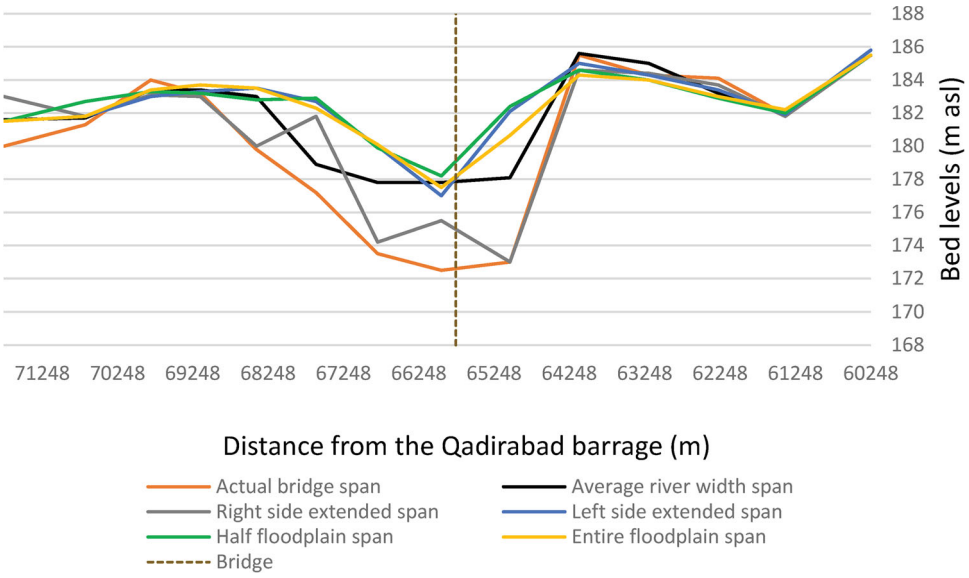

Figure 16. Longitudinal profiles of thalweg elevation were computed for the different scenarios at the end of the simulation period, corresponding to the situation of 31 December 2017.

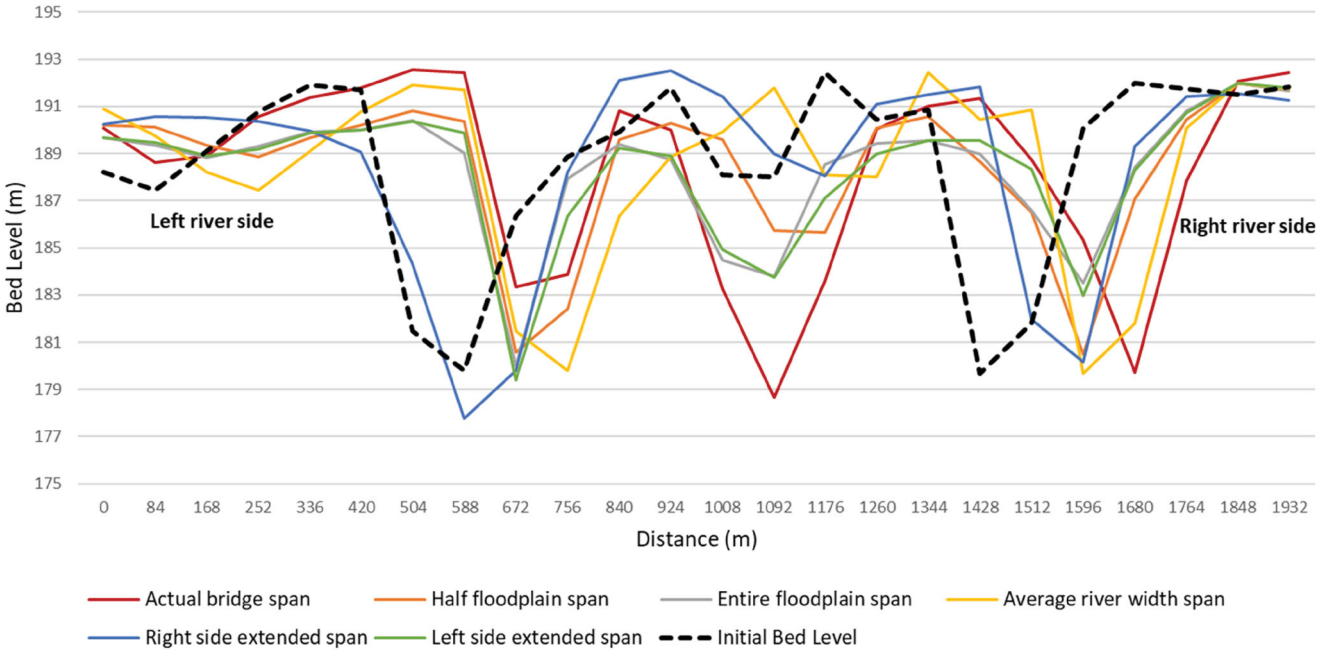

Figure 17. Computed cross-sections 1,486 m downstream of the bridge, seen from upstream. Due to negligible difference scenarios 1 and 2 are not distinguished.

ones obtained with the morphodynamic model (mobile bed) highlights the importance of including morphodynamic changes in flood modelling (Radice et al. 2013; Surian et al. 2016; Nones 2019). Table 4 reports the results for the base-case scenario (actual bridge configuration) at a cross-section located upstream of the bridge, at a distance of 1,588 m. The hydrodynamic model, with fixed bed, does not consider the bed erosion that occurs during high flows and systematically computes higher flood levels (Wiejaczka 2016; Singha et al. 2020).

The results of the morphodynamic computations also show that despite the flood discharge in 2016 was higher than the one in 2013, the 2016 event produced lower water levels (Table 4). This can be attributed to the incorporation of bed level changes in the modelling process, which included the morphological effects of the flood event of 2014 consisting of bed erosion at

Table 4. Water levels during floods for the actual bridge configuration were computed with the morphodynamic model (mobile bed) and with the hydrodynamic model (fixed bed) upstream of the bridge, at a distance of 1,588 m.

Date	Discharge (m^3/s)	Fixed Bed (m asl)	Mobile Bed (m asl)	Difference (m)
8-Aug-2010	8464	196.1	193.8	2.3
16-Aug-2013	10147	196.8	194.25	2.55
7-Sep-2014	21917	200.2	196.6	3.6
8-Aug-2016	11481	197.73	193.35	7.38

the bridge section. The deeper channel provided additional space to the subsequent flood event of 2016. This signifies that the traditional fixed-bed modelling approaches might not be accurate enough (Marco 1994; Ramirez et al. 2016) and might lead to misguided risk awareness (Vázquez-Tarrío et al. 2024). Hence, accurate estimation of flood water levels and inundation extents requires incorporating bed level changes (Guan et al. 2015), even those caused by previous flood events. This is true especially for quickly responding sand-bed rivers, as for example our study case and the Pilcomayo River (Martín-Vide et al. 2019; Crosato et al. 2022). The results of the studies by Hou et al. (2016), Reisenbüchler et al. (2019), Guan et al. (2015), Contreras and Escauriaza (2020) and Tu et al. (2020) confirm the results of this study, which, although based on a specific case-study, can therefore be generalized for applications to other large sand-bed rivers.

At bridge crossings and immediately downstream, the most prominent morphological change is bed erosion (Rashid and Habib 2022). Upstream, bed aggradation and bar formation deviate from the main flow, cause local bank erosion and bend growth (Gaillot and Piegay 1999), as well as water level rise (Grove James et al. 2013). Sediment deposition occurs especially downstream of bridge crossings, where the flow exiting the narrow portion suddenly decelerates. Both upstream and downstream, bar formation creates eddies and vortices due to variations in velocity and pressure. These locally increase the entrainment of bed material, contributing to localized bed and bank erosion (Unsworth et al. 2020). These results agree with the study of Uddin et al. (2022).

Bank retreat is the result of fluvial sediment entrainment, as well as mass failure. Depending on channel geometry and bank material, fluvial entrainment can be less significant than mass failure. In the study area, bank retreat takes place mainly in the form of wedge failure and the material accumulated at the toe of the bank is soon washed away by the flow, quickly making the bank slope steep and instable again (Best et al. 2003).

In general, bank failure occurs during flood recession (Rinaldi and Casagli 1999; Rinaldi et al. 2004), because the saturated weight of the wedge is not balanced by the hydrostatic pressure anymore. Hence, in numerical models, fluvial erosion should be coupled with mass failure and include the effect of pore water pressure on the angle of repose (Rinaldi et al. 2008). However, in the version of Delft 3D used for this study (V4), bank erosion is only computed along wet-dry cell margins by assigning a fraction of bed erosion in a wet cell to the adjacent dry cell, which then becomes wet and (numerically) active. During high flows, the margin between wet and dry cells shifts away from the maximum bed erosion sections of the river, causing an underestimation of the main channel bank retreat. Increasing the fraction of bed erosion to be assigned to adjacent dry cells is not a solution to this problem. Parsapour-Moghaddam et al. (2023) have recently extended the physical description of bank erosion in Delft3D, which they do not limit to dry cells adjacent to wet cells. Based on the angle of repose exceedance between two cells, erosion is assigned to the cell with higher bed elevation in a way that is proportional to the local bed load rate. Using this method should be more efficient in reproducing bank erosion during floods when the main channel and floodplains are all wet.

River banks can be engineered to control channel shift and bank slope. Dave and Mittelstet (2017) compared several bank erosion-control practices in terms of efficiency and cost-effectiveness and found that retaining walls and rip-rap were valid solutions, but required large investments. Other common practices, such as the construction of jetties and rock toe, require fewer capital investments but have higher rates of failure. Hamidifar et al. (2018) demonstrated that certain types of vegetation, such as Vetiver Grass, can be used as a bioengineering tool for erosion control and slope stabilization for a long period, indicating a more nature-friendly way to control river banks. On the same line, Azarisamani et al. (2020) showed that vegetation on bank slopes might indeed have a significant effect by decreasing near-bank flow velocity and turbulence. However, nature-based solutions depend on river size and dynamics and should be carefully studied. For instance, Duró et al. (2020) show that trees on river banks do not prevent bank erosion in the middle-sized Meuse River.

The development of channel bifurcations is another important morphological development related to the

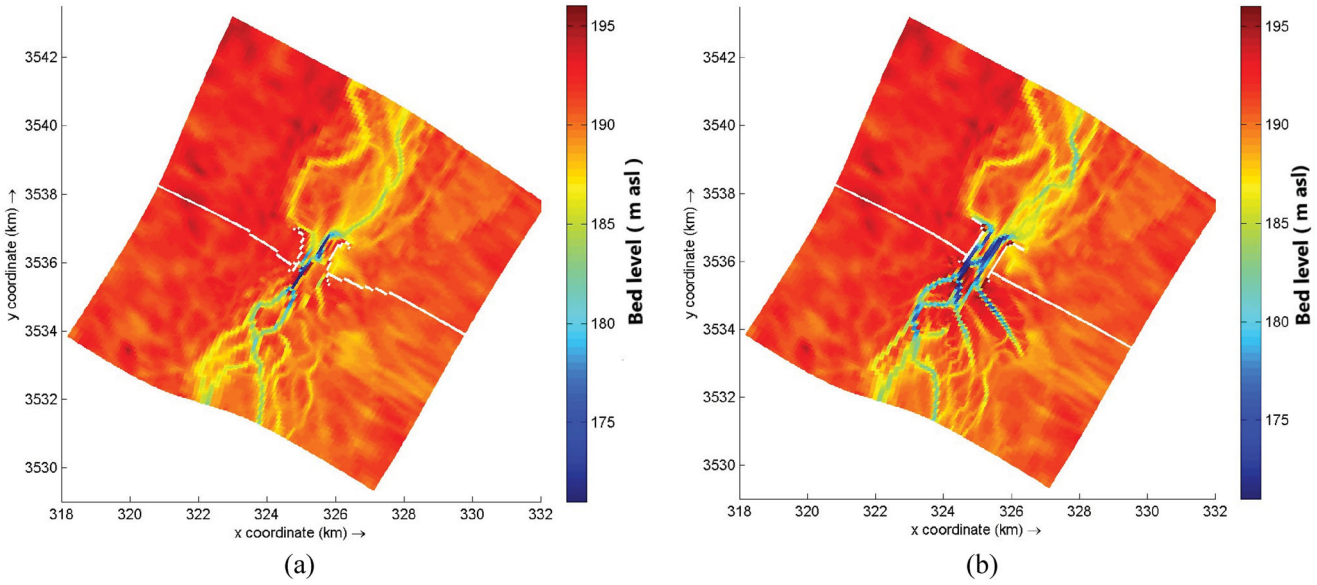

Figure 18. Computed bed elevation in 2021 (computational period 2010–2021). (A) with the bridge forming an angle of 20 degrees with the river channel alignment. (B) with the bridge perpendicular to the river channel.

construction of bridges (Lu et al. 2022). Our study shows that this depends on bridge configuration. The creation of new channels is especially prominent in the base-case (scenarios 1 and 2) with the smallest bridge span, followed by the right-side extended-span case (scenario 4). Despite the widening of the bridge span at this side, the higher floodplain does not offer space for the flow, so in practice, scenario 4 resembles the base-case. Bifurcating channels are also deeper and bars grow higher in these scenarios. Higher sediment supplies from bed erosion at the bridge crossing, due to higher flow velocity in the narrower reach, enhances channel splitting. This is due to higher sediment deposition and bar formation downstream of the bridge where the flow suddenly decelerates, which progressively cause the flow to divide (Cyples et al. 2020). These major morphological changes occur during high flows (Saleem et al. 2020). Scenarios 1, 2 and 4 present also the creation of a deeper diagonal channel across the vast bar downstream of the bridge (Nandi et al. 2022; Li et al. 2023). This is due to the difference in water levels between parallel channels caused by variations in water depth and flow resistance, which creates a gradient in transverse direction (Schuurman and Kleinhans 2015). As soon as the gradient drops farther downstream, the number of splits decreases and the splitting channels become shallower. In the base-case (scenarios 1 and 2), the stream flow also carves a channel through the floodplain section at the left side of the river.

A shortcoming of our numerical study is not considering the effects of bridge piles. This is due to the fact that bridge piles are sub-grid structures, difficult to incorporate in a large-scale model. Bridge piles influence the water flow and the locations where scour and bars form. Moreover, piles increase the water resistance and thus the backwater effects of bridges. However, the location and size of bridge piles are much case-dependent and considering them would diminish the generality of the study, considering also that the study focuses on large-scale effects.

The numerical model covered a period of 8 years, showing that a bridge together with guide bunds can be regarded as channel narrowing and that the impact of these structures becomes prominent during high-flow events (Candel et al. 2021). In the long-term channel narrowing can be expected to cause bed erosion also upstream, which depends on the length of the narrowed reach and longitudinal bed slope of the river. In the study site, narrowing occurs for a length of 1,200 m and the slope is 0.32 m/km, which indicates that bed erosion upstream will be rather limited (Jansen et al. 1979).

The results show that the span location across the floodplain is an important factor for the morphodynamic impact of bridges. In our study, the equally long spans extended either to the right or the left side of the river (scenarios 4 and 5) exhibited different water levels. The former experienced higher water levels and was closer to the scenario with an average river width span because the floodplain bed level is higher on the right side and more resistant to erosion, which prevented local channel widening. This shows that span extension alone is not sufficient to lower upstream flooding, but floodplain topography is also an important factor.

The simplicity of the bridge geometry used in the modelling process does not allow for detailed generalization of the results. In reality, bridges are not exactly perpendicular to the water flow and guide bunds may have different orientations. To show the effects of a different bridge orientation, the calibrated model was run once again with a bridge alignment forming an angle of 20 degrees with the river channel. The computed river morphology is now closer to the observed one since this is in fact the actual alignment of the Talibwala Bridge, which is another indication of the validity of the adopted model. The forced bar emerging at the left side of the bridge in the real situation (Figure 1) is now reflected in the computational results (Figure 18(a)), which shows that the emergence of this forced bar can be attributed to the geometry of the bridge rather than to the presence of dumped debris. Downstream of the bridge, the channel splits into two channels with a central bar dividing them, which is also visible in Figure 1. The number of splits downstream of the bridge appears influenced by bridge alignment too. With a bridge perpendicular to the flow, the splits are more numerous (Figure 18(b)) than with the 20-degree angle (Figure 18(a)). Since this study did not consider more scenarios with different bridge alignments, its results can be considered applicable only to bridges that are perpendicular to the river flow. However, our findings suggest that bridge alignment might play a significant role in the morphological impact of bridges and should be carefully considered in the design phase of bridges.

Conclusion and recommendations

Bridges can have a significant impact on river morphology and water levels because they reduce the flow width during flood events. Upstream of bridges, observed morphological changes include bar formation and bank erosion. Downstream of bridges, we find bed and bank erosion, especially close to the structure. We studied the hydrodynamic and morphodynamic effects of bridges crossing a wide sand-bed river. The original aspect of this research lies in the use of a physics-based 2D morphological model that allowed assessing the factors governing the formation of bars upstream and downstream of a bridge, as well as bank erosion, for several bridge configurations. The major factor causing bar growth appears to be the bridge span (the larger the span the less bar growth). Another important factor is bridge alignment with respect to the river flow. The results of the model indicate that non-perpendicularity can lead to the formation of larger bars both upstream and downstream of the structure. The location of the bridge openings across the floodplain might influence the morphodynamic response too, in particular, if there are physical and topographic differences in the floodplain resulting in higher or lower flood conveyance. It is important to notice that bar formation is the major cause of bank erosion leading to local channel shift, both upstream and downstream of the structure.

The results of this work also show that the greater the span of the bridge, the lower its hydro-morphodynamic impact. In particular, larger bridge spans reduce backwater effects and thus high-flow levels upstream. In the study area, the backwater length has an order of magnitude of 70 km, of which the first 17 kilometres are the most affected. This means that in wide sand-bed rivers, like the Chenab, the effects of a bridge can be felt rather far upstream. Larger bridge spans produce also less bed erosion in the area just downstream of the structure, as well as less bank erosion, both in the upstream and downstream directions.

The findings of this work are specifically applicable to wide sand-bed rivers with hydraulic and morphological characteristics similar to the Chenab and are supported by previous studies focusing on specific river crossing cases. However, considering that the observed processes occur also in other types of rivers, the detected trends can be considered general. The extent and magnitude of morphological changes, however, depend on factors such as bridge geometry, discharge variations, and sediment characteristics and are case-specific.

The results of this research can guide future bridge constructions and modifications to existing bridges across large sand-bed rivers. Extending the span of existing bridges that cause hydro-morphodynamic problems, especially during and after high-flow events, can be regarded as an efficient impact-mitigation measure. It can reduce the risk of flooding in the upstream area affected by backwater, which can be tens of kilometres long, as well as bed and bank erosion in the vicinity of the bridge. When assessing the hydro-morphological effects of different bridge spans, however, designers should also consider the topography of the floodplain to determine the optimum location of the extension. River bed deepening and bank erosion should be considered for bridge pillar foundations and for the protection of agricultural land and settlements near river banks. Finally, the results of this study emphasize the importance of using morphodynamic instead of hydrodynamic models for accurate flood level assessments.

Acknowledgements

The authors are thankful to the Punjab Irrigation Department of the Ministry of Water Resources, Pakistan, that funded the

research. The authors are also grateful to Prof. Micha Werner for his useful suggestions.

Data availability statement

All data, models, and code generated or used during the study appear in the submitted article.

References

AA Planners and Consulting Engineers. 2021. Talibwala bridge over river chenab. https://www.aa-associates.com/bridge-design-survey-consultancy-supervision/talibwala-bridge-over-river-c.html

Abdou A, Valero D, Crosato A. 2021. Large-scale morphodynamic impact of groups of piers on low-land rivers. International Junior Researcher and Engineer Workshop on Hydraulic Structures. https://digitalcommons.usu.edu/ewhs/2021/Session1/4/

Alam JB, Uddin M, Ahmed JU, Cacovean H, Rahman HM, Banik BK, Yesmin N. 2007. Study of morphological change of river old Brahmaputra and its social impacts by remote sensing. Geographia Technica. 2:1–11. https://www.academia.edu/download/53749833/gt_2_2007.pdf

Ali S, Cheema MJM, Waqas MM, Waseem M, Leta MK, Qamar MU, Awan UK, Bilal M, Rahman MHU. 2021. Flood mitigation in the transboundary Chenab river basin: a basin-wise approach from flood forecasting to management. Remote Sens. 13(19):3916. doi:10.3390/rs13193916.

Ashraf M, Shakir AS. 2018. Prediction of river bank erosion and protection works in a reach of Chenab river, Pakistan. Arab J Geosci. 11:145. doi:10.1007/s12517-018-3493-7.

Azarisamani A, Keshavarzi A, Hamidifar H, Javan M. 2020. Effect of rigid vegetation on velocity distribution and bed topography in a meandering river with a sloping bank. Arab J Sci Eng. 45(10):8633–8653. doi:10.1007/s13369-020-04818-7.

Azhar F. 2018. Morphodynamic Changes Around a Bridge Pier [Msc Thesis WSE-HERBD-18.03]. IHE Delft Institute for Water Education, Delft, the Netherlands, downloadable from: https://ihedelftrepository.contentdm.oclc.org/digital/api/collection/masters2/id/1237/download

Bélanger JB. 1841. Notes sur l'Hydraulique (Notes on Hydraulic Engineering). Ecole Royale des Ponts et Chaussées. Paris, France. Session 1841-1842, 223.

Best JL, Ashworth PJ, Bristow CS, Roden J. 2003. Three-dimensional sedimentary architecture of a large, mid-channel sand braid bar, Jamuna River, Bangladesh. J Sediment Res. 73(4):516–530. doi:10.1306/010603730516.

Bhuiyan M, Rakib M, Takashi K, Rahman M, Suzuki S. 2010. Regulation of Brahmaputra-jamuna river around Jamuna bridge site, Bangladesh: geoenvironmental impacts. J Water Resource Prot. 2(2):123–130. doi:10.4236/jwarp.2010.22014.

Biswas M, Banerjee P. 2018. Bridge construction and river channel morphology - a comprehensive study of flow behavior and sediment size alteration of the River Chel, India. Arab J Geosci. 11:467. doi:10.1007/s12517-018-3789-7.

Biswas SS, Pal R, Pramanik MK, Mondal B. 2015. Assessment of anthropogenic factors and floods using remote sensing and GIS on lower regimes of Kangshabati-Rupnarayan River Basin, India. Int J Remote Sens GIS. 4(2):77–86. https://www.academia.edu/download/111067062/RSG4204.pdf

Candel J, Kleinhans M, Makaske B, Wallinga J. 2021. Predicting river channel pattern based on stream power, bed material and bank strength. Prog Phys Geogr. 45(2):253–278. doi:10.1177/0309133320948831.

Chohan K, Ahmad SR, Ashraf A, Kamran M, Rasheed R. 2022. Remote sensing based innovative solution of river morphology for better flood management. Int J Appl Earth Obs Geoinf. 111:102845. doi:10.1016/j.jag.2022.102845.

Contreras MT, Escauriaza C. 2020. Modeling the effects of sediment concentration on the propagation of flash floods in an andean watershed. Nat Hazards Earth Syst Sci. 20(1):221–241. doi:10.5194/nhess-20-221-2020.

Costabile P, Macchione F, Natale L, Petaccia G. 2014. Representing skewed bridge crossing on 1-D and 2-D flood propagation models: compared analysis in practical studies. Proceedings of the International Conference on Fluvial Hydraulics, RIVER FLOW. 733–741.

Crosato A, Grissetti-Vázquez A, Bregoli F, Franca MJ. 2022. Adaptation of river channels to a wetter or drier climate: insights from the lower Pilcomayo River, South America. J Hydrol. 612(C):128254. doi:10.1016/j.jhydrol.2022.128254.

Crosato A, Mosselman E. 2020. An integrated review of river bars for engineering, management and transdisciplinary research. Water. 12(2):596. doi:10.3390/w12020596.

Cyples NN, Ielpi A, Dirszowsky RW. 2020. Planform and stratigraphic signature of proximal braided streams: remote-sensing and ground-penetrating-radar analysis of the Kicking Horse River, Canadian Rocky Mountains. J Sediment Res. 90(1):131–149. doi:10.2110/jsr.2020.6.

Dave N, Mittelstet AR. 2017. Quantifying effectiveness of streambank stabilization practices on Cedar River, Nebraska. Water. 9(12):930. doi:10.3390/w9120930.

Deltares. 2023. Delft3D-FLOW, user manual: simulation of Multi-Dimensional Hydrodynamic Flows and Transport Phenomena, Including Sediments. Delft, The Netherlands: Deltares. https://content.oss.deltares.nl/delft3d4/Delft3D-FLOW_User_Manual.pdf

Duró G, Crosato A, Kleinhans MG, Winkels TG, Woolderink HAG, Uijttewaal WSJ. 2020. Distinct patterns of bank erosion in a navigable regulated river. Earth Surf Process Landforms, 45(2):361–374. doi:10.1002/esp.4736.

Dysarz T, Kałuża T, Mickevičius K, Veigneris J, Zawadzki P, Kujawiak S, Zaborowski S, Wicher-Dysarz J, Baublys R, et al. 2023. Application of physical and numerical modeling for determination of waterway safety under the bridge in Kaunas City, Lithuania. Water. 15(4):731. doi:10.3390/w15040731.

Engelund F, Hansen E. 1967. A monograph on sediment transport in alluvial streams. *Technical University of Denmark 0stervoldgade 10, Copenhagen K*.

Flokstra C, Koch F. 1981. Numerical Aspects of bed Level Predictions for Alluvial River Bends. Delft, Netherlands: WL Delft Hydraulics Laboratory. Publication 258.

Flood Forecasting Division (FFD), L. 2023. River's maximum observed peaks discharge. https://ffd.pmd.gov.pk/ffd_others/hpeak.htm

Gaillot S, Piegay H. 1999. Impact of gravel-mining on stream channel and coastal sediment supply: example of the Calvi Bay in Corsica (France). J Coast Res. 15(3):774–788. https://www.jstor.org/stable/4298991

Grove James R, Croke J, Thompson C. 2013. Quantifying different riverbank erosion processes during an extreme flood event. Earth Surf Process Landf. 38(12):1393–1406. doi:10.1002/esp.3386.

Guan M, Wright NG, Sleigh PA, Carrivick JL. 2015. Assessment of hydro-morphodynamic modelling and geomorphological impacts of a sediment-charged jökulhlaup, at Sólheimajökull, Iceland. J Hydrol. 530:336–349. doi:10.1016/j.jhydrol.2015.09.062.

Gumbel EJ. 1941. The return period of flood flows. Ann Math Stat. 12(2):163–190. doi:10.1214/aoms/1177731747.

Hager WH, Unger J. 2010. Bridge pier scour under flood waves. J Hydraul Eng. 136(10):842–847. doi:10.1061/(asce)hy.1943-7900.0000281.

Hamidifar H, Keshavarzi A, Truong P. 2018. Enhancement of river bank shear strength parameters using vetiver grass root system. Arab J Geosci. 11:611. doi:10.1007/s12517-018-3999-z.

Hou J, Li Z, Liang Q, Li G, Cheng W, Wang W, Wang R. 2016. Effects of morphological change on fluvial flood patterns evaluated by a hydro-geomorphological model. Procedia Eng. 154:441–449. doi:10.1016/j.proeng.2016.07.536.

Hu Y, Yang H, Zhou H, Lv Q. 2023. A review of numerical modelling of morphodynamics in braided rivers: mechanisms, insights and challenges. Water. 15(3):595. doi:10.3390/w15030595.

Islam MT. 2013. Time series landsat remote sensing images and geographical information system to environmental evaluation of sites for the Padma river bridge. Int J Remote Sens GIS. 2(3):114–121. https://www.bip.org.bd/admin/uploads/member-publication/2013/MP–1772fdf5c5.pdf

Jansen P, Van Bendegom L, Van Den Berg JH, De Vries MB, Zanen A. 1979. Principles of river engineering: the non-tidal Alluvial River. Delft: Delftse Uitgevers Maatschappij BV.

Laursen EM. 1970. Bridge design considering scour and risk. J Transp Eng. 96(2):149–164. doi:10.1061/tpejan.0000079.

Lee KT, Ho Y-H, Chyan Y-J. 2006. Bridge blockage and overbank flow simulations using HEC–RAS in the Keelung river during the 2001 nari typhoon. J Hydraul Eng. 132(3):319–323. doi:10.1061/(asce)0733-9429(2006)132:3(319).

Lesser GR, Roelvink JA, van Kester JATM, Stelling GS. 2004. Development and validation of a three-dimensional morphological model. Coast Eng. 51(8-9):883–915. doi:10.1016/j.coastaleng.2004.07.014.

Li W, Colombera L, Yue D, Mountney NP. 2023. Controls on the morphology of braided rivers and braid bars: An empirical characterization of numerical models. Sedimentology. 70(1):259–279. doi:10.1111/sed.13008.

Lu H, Li Z, Hu X, Chen B, You Y. 2022. Morphodynamic processes in a large gravel-bed braided channel in response to runoff change: a case study in the source region of Yangtze river. Arab J Geosci. 15(5):377. doi:10.1007/s12517-022-09641-y.

Mahmud MI, Mia AJ, Islam MA, Peas MH, Farazi AH, Akhter SH. 2020. Assessing bank dynamics of the lower Meghna river in Bangladesh: an integrated GIS-DSAS approach. Arab J Geosci. 13:602. doi:10.1007/s12517-020-05514-4.

Marco JB. 1994. Flood risk mapping. In: Rossi, G. et al, (eds.). Coping with Floods. Dordrecht: Springer Netherlands; p. 353–373. doi:10.1007/978-94-011-1098-3_20.

Martín-Vide JP, Capape S, Ferrer-Boix C. 2019. Transient scour and fill. The case of the Pilcomayo river. J Hydrol. 576:356–369. doi:10.1016/j.jhydrol.2019.06.041.

McFeeters SK. 2013. Using the normalized difference water index (NDWI) within a geographic information system to detect swimming pools for mosquito abatement: a practical approach. Remote Sens. 5(7):3544–3561. doi:10.3390/rs5073544.

Mueller JR. 1968. An introduction to the hydraulic and topographic sinuosity indexes. Ann Am Assoc Geogr. 58(2):371–385. doi:10.1111/j.1467-8306.1968.tb00650.x.

Nandi KK, Pradhan C, Padhee SK, Dutta S, Khatua KK. 2022. Understanding the entropy-based morphological variability and energy expenditure mechanism of a large braided river system. J Hydrol. 615(A):128662. doi:10.1016/j.jhydrol.2022.128662.

National Engineering Services Pakistan. 2010. Gradation curve for River Chenab sand, NESPAK central library, Lahore. http://www.nespak.com.pk/

Nones M. 2019. Dealing with sediment transport in flood risk management. Acta Geophysica. 67:677–685. doi:10.1007/s11600-019-00273-7.

Ogras S, Onen F. 2020. Flood analysis with HEC-RAS: a case study of Tigris river. Adv Civ Eng. 2020:6131982. doi:10.1155/2020/6131982.

Oo MM, Kyi CCT, Zin WW. 2019. Historical morphodynamics assessment in bridge areas using remote sensing and GIS techniques. Civ Eng J. 5(11):2515–2524. doi:10.28991/cej-2019-03091429.

Panjab Irrigation Department. 2023. Daily river discharge data. https://irrigation.punjab.gov.pk/dynamic-line-diagram

Parsapour-Moghaddam P, Rennie CD, Slaney J, Platzek F, Shirkhani H, Jamieson E, Mosselman E, Measures R. 2023. Implementation of a new bank erosion model in Delft3D. J Hydraul Eng ASCE. 149(10):04023038. doi:10.1061/JHEND8.HYENG-13206.

Radice A, Rosatti G, Ballio F, Franzetti S, Mauri M, Spagnolatti M, Garegnai G. 2013. Management of flood hazard via hydro-morphological river modelling. The case of the mallero in Italian Alps. J Flood Risk Manag. 6(3):197–209. doi:10.1111/j.1753-318x.2012.01170.x.

Ramirez JA, Lichter M, Coulthard TJ, Skinner C. 2016. Hyper-resolution mapping of regional storm surge and tide flooding: comparison of static and dynamic models. Natural Hazards. 82(1):571–590. doi:10.1007/s11069-016-2198-z.

Rashid MB, Habib MA. 2022. Channel bar development, braiding and bankline migration of the Brahmaputra-Jamuna river, Bangladesh through RS and GIS techniques. Int J River Basin Manage. 22(2):203–215. doi:10.1080/15715124.2022.2118281.

Rasool S, Rana IA, Ahmad S. 2022. Linking flood risk perceptions and psychological distancing to climate change: a case study of rural communities along Indus and Chenab rivers, Pakistan. Int J Disaster Risk Reduct. 70:102787. doi:10.1016/j.ijdrr.2022.102787.

Reisenbüchler M, Bui MD, Skublics D, Rutschmann P. 2019. An integrated approach for investigating the correlation between floods and river morphology: a case study of the Saalach river, Germany. Sci Total Environ. 647:814–826. doi:10.1016/j.scitotenv.2018.08.018.

Rinaldi M, Casagli N. 1999. Stability of streambanks formed in partially saturated soils and effects of negative pore water pressure: the Sieve river (Italy). Geomorphology. 26(4):253–277. doi:10.1016/S0169-555X(98)00069-5.

Rinaldi M, Casagli N, Dapporto S, Gargini A. 2004. Monitoring and modelling of pore water pressure changes and riverbank stability during flow events. Earth Surf Process Landf. 29:237–254. doi:10.1002/esp.1042.

Rinaldi M, Mengoni B, Luppi L, Darby SE, Mosselman E. 2008. Numerical simulation of hydrodynamics and bank erosion in a river bend. Water Resour Res. 44(9):W09428. doi:10.1029/2008wr007008.

Saleem A, Dewan A, Rahman MM, Nawfee SM, Karim R, Lu XX. 2020. Spatial and temporal variations of erosion and accretion: A case of a large tropical river. Earth Syst Environ. 4:167–181. doi:10.1007/s41748-019-00143-8.

Schuurman F, Kleinhans MG. 2015. Bar dynamics and bifurcation evolution in a modelled braided sand-bed river. Earth Surf Process Landf. 40(10):1318–1333. doi:10.1002/esp.3722.

Siddiqui MJ, Haider S, Gabriel HF, Shahzad A. 2018. Rainfall–runoff, flood inundation and sensitivity analysis of the 2014 Pakistan flood in the Jhelum and Chenab river basin. Hydrolog Sci J. 63(13-14):1976–1997. doi:10.1080/02626667.2018.1546049.

Singh U, Crosato A, Giri S, Hicks M. 2017. Sediment heterogeneity and mobility in the morphodynamic modelling of gravel-bed braided rivers. Adv Water Resour. 104:127–144. doi:10.1016/j.advwatres.2017.02.005.

Singha P, Das P, Talukdar S, Pal S. 2020. Modeling livelihood vulnerability in erosion and flooding induced river island in Ganges riparian corridor, India. Ecol Indic. 119:106825. doi:10.1016/j.ecolind.2020.106825.

Surian N, Righini M, Lucía A, Nardi L, Amponsah W, Benvenuti M, Borga M, Cavalli M, Comiti F, Marchi L, et al. 2016. Channel response to extreme floods: insights on controlling factors from six mountain rivers in Northern Apennines, Italy. Geomorphology. 272:78–91. doi:10.1016/j.geomorph.2016.02.002.

Tu H, Wang X, Zhang W, Peng H, Ke Q, Chen X. 2020. Flash flood early warning coupled with hydrological simulation and the rising rate of the flood stage in a mountainous small watershed in Sichuan province, China. Water. 12(1):255. doi:10.3390/w12010255.

Uddin MJ, Haque MN, Fayshal MA, Dakua D. 2022. Assessing the bridge construction effect on river shifting characteristics through geo-spatial lens: a case study on Dharla river, Bangladesh. Heliyon. 8(8):e10334. doi:10.1016/j.heliyon.2022.e10334.

Unsworth CA, Nicholas AP, Ashworth PJ, Best JL, Lane SN, Parsons DR, Sambrook Smith GH, Simpson CJ, Strick RJP. 2020. Influence of dunes on channel-scale flow and sediment transport in a sand bed braided river. J Geophys Res Earth Surf. 125(11):e2020JF005571. doi:10.1029/2020jf005571.

Vázquez-Tarrío D, Ruiz-Villanueva V, Garrote J, Benito G, Calle M, Lucía A, Díez-Herrero A. 2024. Effects of sediment transport on flood hazards: lessons learned and remaining challenges. Geomorphology. 446:108976. doi:10.1016/j.geomorph.2023.108976.

Villada Arroyave JA, Crosato A. 2010. Effects of river floodplain lowering and vegetation cover. Proc Ins Civ Eng-Water Manage. 163(9):457–467. doi:10.1680/wama2010.163.11.

Wiejaczka Ł. 2016. Riverbeds level changes in the margin and foreland of the Darjeeling Himalaya during the years with a normal monsoon rainfall. In: Singh R., Prokop P., editor. *Environmental geography of South Asia.* Advances in geographical and environmental sciences. Tokyo: Springer; p. 83–95. doi:10.1007/978-4-431-55741-8_5.